FISEVIER

Contents lists available at ScienceDirect

## **Quaternary Science Reviews**

journal homepage: www.elsevier.com/locate/quascirev



# Multi-proxy stalagmite records from northern California reveal dynamic patterns of regional hydroclimate over the last glacial cycle



Jessica L. Oster <sup>a, \*</sup>, Isabelle E. Weisman <sup>a</sup>, Warren D. Sharp <sup>b</sup>

- <sup>a</sup> Department of Earth and Environmental Sciences, Vanderbilt University, Nashville, TN, 37240, USA
- <sup>b</sup> Berkeley Geochronology Center, Berkeley, CA, 94709, USA

#### ARTICLE INFO

Article history: Received 28 January 2020 Received in revised form 2 June 2020 Accepted 3 June 2020 Available online xxx

Keywords: Speleothems Paleoclimatology Quaternary North America

## ABSTRACT

Despite its importance for California's water resources, little is known about how precipitation has varied in far northern California beyond the historical record. We present a new, multi-proxy paleoclimate record derived from two coeval stalagmites from Lake Shasta Caverns (LSC), California that covers the end of Marine Isotope Stage 3 through Heinrich Stadial 1 (~35,000 to 14,000 years BP). At 40.8°N, LSC is situated within the transition zone between regions in the northwestern and southwestern United States that demonstrate different precipitation responses to both modern and paleoclimatic drivers. Stable isotope and trace element proxies from LSC stalagmites indicate the region experienced wet conditions during interstadials (warm periods) associated with Dansgaard-Oeschger cycles, similar to proxy records from southern Oregon and the northern Great Basin, but in contrast to records from the desert southwest. Similar to the northern Cascades and Rocky Mountains, LSC was drier during the Last Glacial Maximum, However, proxies indicate increased rainfall throughout Heinrich Stadial 1, similar to the Great Basin and southwest. Thus, the LSC record demonstrates the non-stationarity of the transition zone location and illustrates a complex pattern of precipitation response to global climate change in the western United States. Covariation of speleothem  $\delta^{18}$ O, an indicator of moisture source, with  $\delta^{13}$ C and trace elements, indicators of moisture amount, suggest a higher proportion of Central Pacific precipitation during the Last Glacial Maximum, despite the enhanced aridity. In contrast, periods characterized by increased precipitation amounts, such as early Heinrich 1, are associated with enhanced moisture from the Northern Pacific.

© 2020 Elsevier Ltd. All rights reserved.

#### 1. Introduction

Proxy evidence supports a dynamic hydroclimate across western North America during the last glacial period and deglaciation. Regional proxy compilations illustrate the spatial pattern of hydroclimatic variability in response to the climate of the Last Glacial Maximum (LGM) ~21,000 yrs BP (Thompson et al., 1993; Bartlein et al., 2011; Oster et al., 2015a; Scheff et al., 2017). Comparisons of terrestrial proxy time series reveal hydroclimatic shifts at millennial and longer time scales, providing evidence for coherent but potentially complex changes during the last deglaciation (Oster and Kelley, 2016; Feakins et al., 2019) and earlier during Marine Isotope Stages 3–5 in response to Dansgaard-Oeschger cycles (Benson et al., 2013; Glover et al., 2017). Comparisons of

the timing of pluvial lake highstands and other proxy records have revealed complex regional patterns arising from forcings such as the growth and decay of the Laurentide Ice Sheet, variations in Atlantic Meridional Overturning Circulation, interhemisphere temperature gradients, and the position of the Intertropical Convergence Zone that influence the amount and sources of moisture reaching western North America (Oster et al., 2015a; Morrill et al., 2018; Asmerom et al., 2017; McGee et al., 2018; Hudson et al., 2019). The relative importance of these drivers on different time scales remains a source of active investigation.

Presently, winter precipitation in western North America has been shown to exhibit a north/south, wet/dry dipole pattern on interannual to decadal timescales partly in response to ocean-atmosphere interactions across the Pacific and Atlantic Oceans including the El Niño/Southern Oscillation, the Pacific Decadal Oscillation, and the Atlantic Multidecadal Oscillation (Redmond and Koch, 1991; Wise, 2010). This dipole pattern is associated with both the distribution of total rainfall across the region as well

<sup>\*</sup> Corresponding author.

E-mail address: jessica.l.oster@vanderbilt.edu (J.L. Oster).

as extreme precipitation events (Dettinger et al., 1998; Jiang et al., 2013). Analysis of tree ring records from across western North America suggests that the transition between wet and dry dipole regions has remained consistently centered around 40°N for the past 500 years (Wise, 2016). A geographically similar dipole pattern is evident in regional hydroclimate variations during the LGM in response to the influence of the Laurentide Ice Sheet on atmospheric circulation (Oster et al., 2015a; Lora et al., 2017). At the LGM. climate models and proxy compilations indicate a transition between wet and dry conditions along the west coast occurred near the California-Oregon border (42 °N) (Oster et al., 2015a). There is further evidence that this dipole pattern persisted during millennial-scale climate oscillations of the last deglaciation (Hudson et al., 2019). However, there are comparatively few paleoclimate records that exist close to the location of this dipole transition zone that possess the potential to track changes in the location and behavior of the dipole at different temporal scales.

Here we present a new, U-series dated, multi-proxy speleothem paleoclimate record from Lake Shasta Caverns (LSC) in northern California (40.804°N, 122.304°W). Given its location, LSC is wellsituated to track variations in regional patterns of precipitation change and reveal spatial shifts in the dipole transition zone across the last glacial period and deglaciation (Fig. 1A). We present records of oxygen and carbon isotope and trace element variability in two partly overlapping stalagmites that grew collectively between ~37,000 and 14,000 yrs BP. These combined proxies allow us to explore how changes in moisture source and amount may have influenced the overall hydroclimate at this location and how this variability may have contributed to regional patterns of climate variability during the last glacial period and in response to Dansgaard-Oeschger cycles and Heinrich Events. Our results demonstrate temporal variability in the dipole pattern and highlight the need for multi-proxy records that can parse changes in moisture source versus amount to examine the relative importance of different hydroclimatic drivers for this hydrologically sensitive

## 2. Site and description

Lake Shasta Caverns (LSC) is a commercial cave located approximately 32 km north of Redding, California, on the east side of the McCloud arm of Shasta Lake (40.804°N, 122.304°W, 725 m a.s.l.) (Fig. 1A; B). The cave is developed within the McCloud limestone, which crops out in a north-south belt in the Shasta Lake area (Fig. 1B). The McCloud Limestone is Early Permian in age and ranges in thickness from less than 30 m to about 800 m. It consists mainly of calcarenite composed of varying amounts of crinoid pieces, bryozoans, and fusilinid foraminfera and has been locally dolomitized in places (Demirmen and Harbaugh, 1965). The eastern part of the Shasta Lake area is characterized by a large east-dipping monocline with folds and faults that warp and displace the limestone locally by 600 m or more. In most places, the McCloud Limestone is separated from the underlying Baird Formation (tuffaceous rocks and adjoining sandstones and shales), by a sill of mafic quartz diorite of uneven thickness, and dikes - likely offshoots of the sill – intrude the McCloud in many locations (Demirmen and Harbaugh, 1965).

There are a number of small caves as well as three large cave systems developed in the McCloud Limestone (LSC, Potter Creek, and Samwel Caves). LSC is the largest and most complex cave system of the three. Presently, the cave is accessed through two artificial entrances (marked "Entrance" and "Exit" in Fig. 1C). There is one known natural entrance to the cave that is located approximately 30 m above the Cathedral Room (Fig. 1C; D. Mundt pers. comm). Cave air pCO<sub>2</sub> measured in the winters and summers

(February and June) between 2018 and 2020 ranges from 470 to 696 ppm (average of  $624 \pm 66$  ppm, n=13 across 5 locations) and shows no clear pattern of variation with season or spatially within the cave. Although the artificial entrances are kept closed except when tour groups are exiting and entering the cave, their presence and the tour groups indicate that we cannot straightforwardly extrapolate the pCO<sub>2</sub> of the modern cave atmosphere to the past. However, it is likely that the cave was less well-ventilated before the artificial entrances were put in place.

Cool wet winters and hot, dry summers characterize the climate above LSC. Between 1981 and 2010, Redding, California experienced an average yearly rainfall of 879 mm. Approximately 90% of annual precipitation falls between October and May. The mean annual temperature is 16.8 °C, and ranges from 9.7 °C to 24 °C (US Climate Data). Natural drip-water flow within the cave increases substantially during the winter and spring (up to 5 ml/min) and almost entirely ceases (1–2 drips/min) during the late summer to early fall. During the wet season, drip rates within the cave increase in response to surface rainfall within hours for heavy rainfall, or within a day for more moderate rainfall events (D. Mundt, pers. comm.).

Stalagmites LSC2 and LSC3 were collected in 2006. Both samples were found already broken thus were not active at the time of collection. LSC2 was found in the Cathedral Room and LSC3 was found in the Thompson Room (Fig. 1C). Thus, LSC2 was found closer to, and approximately 110 m below the known natural cave entrance, while LSC3 was found approximately 155 m below the natural entrance. LSC2 is 12 cm tall and consists of dense, non-laminated calcite that is either clear/white or stained brown. LSC3 is ~17.3 cm tall and is also dense calcite, displaying some intervals of silicate-rich banding. (Figs. S1 and S2).

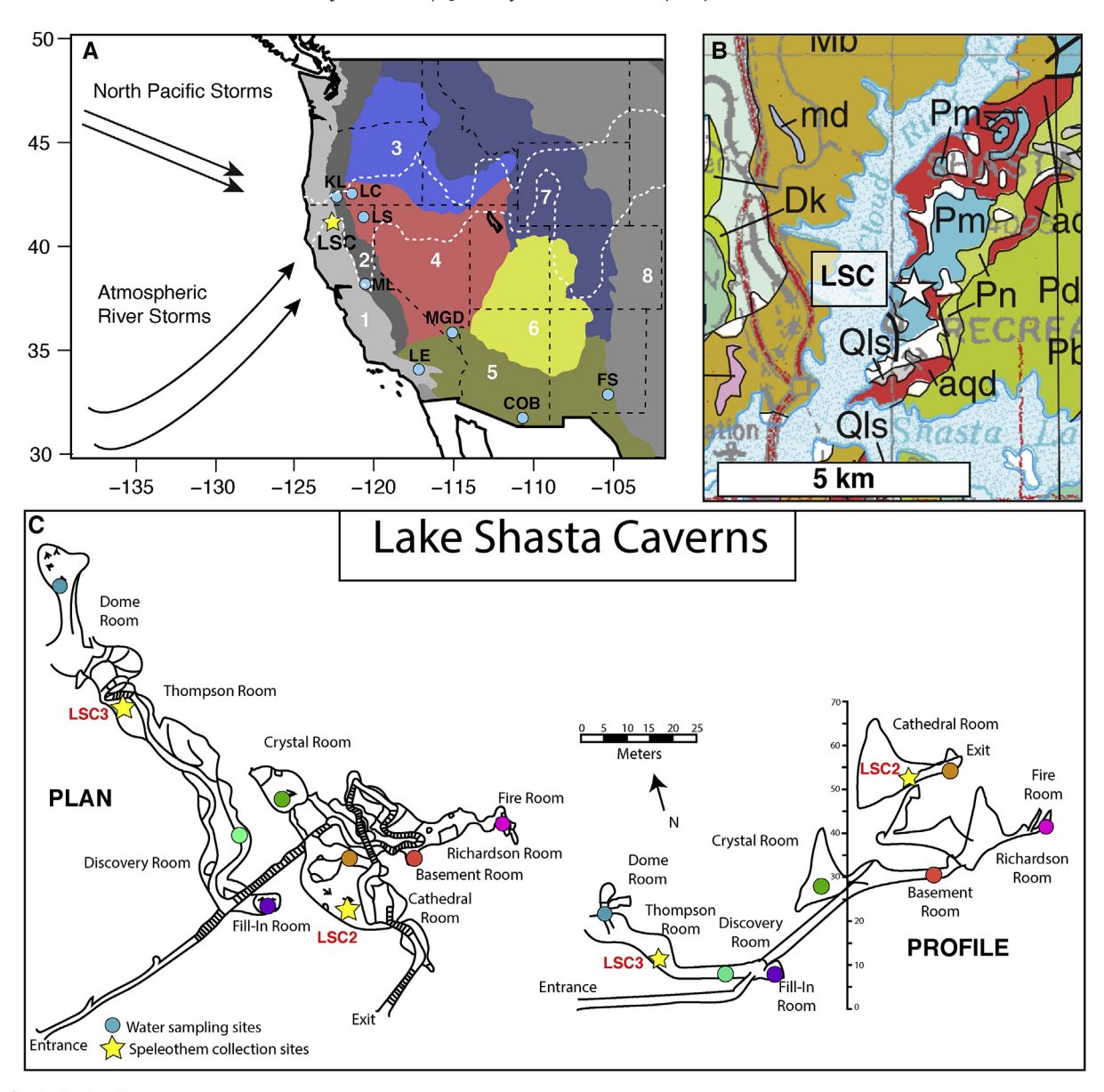
## 3. Methods

#### 3.1. Drip water and precipitation analysis

#### 3.1.1. Water collection and analysis

Through a collaboration with the Lake Shasta Caverns staff, we collected drip water samples at seven locations throughout the cave (Fig. 1C). Three sites have been monitored beginning in December 2015, with water collection at the four other sites beginning at later dates. The drip sites chosen are the most consistently wet locations within the cave. Collections occurred regularly during the cool wet season when drip sites within the cave were more active. Water collections during the summer and fall occurred opportunistically following rainfall events. Water samples for oxygen and hydrogen isotope analysis ( $\delta^{18}$ O,  $\delta^{2}$ H) were collected in precleaned 30 ml LDPE bottles.

To investigate the controls on precipitation  $\delta^{18}O$  and  $\delta^{2}H$  in northern California, we analyzed archived precipitation samples from the National Air Deposition Program (NADP) site CA-76 in Montague, California. CA-76, the closest NADP collection site to the cave, is located approximately 128 km from Lake Shasta Caverns in central northern California (41.7662°N, 122.4798°W, 799 m a.s.l.). Previous work has demonstrated that the NADP collection and archiving protocol successfully preserves water samples for isotopic analysis (Vachon et al., 2010; Berkelhammer et al., 2012). NADP precipitation samples are collected weekly, refrigerated, and archived for ~5 years following collection. We were able to obtain aliquots of rainwater collected between January 2010 and February 2017. Integrated monthly precipitation samples were also collected at LSC following the procedures of Friedman et al. (1992). One-liter Nalgene containers were pre-filled with a 1 cm thick layer of mineral oil to prevent evaporation after precipitation events and covered with a metal mesh filter. Four integrated monthly samples



## Geologic Map Key:

Pm: McCloud Limestone (Pennsylvanian, Permian); Pn: Nosoni Formation (Permian); Pd: Dekkas Andesite (Permian); agd: augite-quartz diorite (Permian); Mbd: Bragdon Formation (Miss.); Mb: Baird formation (Miss. and Penn); Dcg: Copley Greenstone (Devonian); Dk: Kennett Formation (Devonian); mi: mafic intrusive rocks (Jurassic); md: mafic rocks (Permian); Qls: landslide deposits (Holocene);

**Fig. 1.** A) Location of LSC (star). Background map shows western U.S. geographic regions 1. Pacific Border; 2. Cascade-Sierra Mountains; 3. Columbia Plateau; 4. Great Basin; 5. Desert Southwest; 6. Colorado Plateau; 7. Rocky Mountains; 8. Great Plains. Light blue circles show location of proxy records discussed in the text: 1. LC = Summer Lake/Lake Chewaucan (Zic et al., 2002; Hudson et al., 2019); LS = Lake Surprise (Ibarra et al., 2014; Egger et al., 2018); MGD = Mojave groundwater deposits (Springer et al., 2015); KL = Klamath Lake (Bradbury et al., 2004); LE = Lake Elsinore (Feakins et al., 2019); COB = Cave of the Bells (Wagner et al., 2010); FS = Fort Stanton Cave (Asmerom et al., 2010, 2017); ML = McLean's Cave (Oster et al., 2015b). White dashed lines mark the approximate location of the transition zone in the precipitation dipole of (Wise, 2010), characterized by positive (northern) and negative (southern) correlations between modern winter precipitation and the Southern Oscillation Index. B) Geologic map of Lake Shasta area (LSC shown by star) (Fraticelli et al., 2012). C) Map of LSC in plan and profile views (based on unpublished survey data provided by D. Mundt) with locations of drip water samples (circles) and collection locations of stalagmites LSC2 and LSC3 (both found broken). Color of drip water sample locations matches Fig. 2B. (For interpretation of the references to color in this figure legend, the reader is referred to the Web version of this article.)

were collected between December 2015 and March 2016.

Drip water samples were analyzed for  $\delta^{18}$ O and  $\delta^{2}$ H using a Los Gatos Research TWIA-45EP water isotope analyzer at Santa Clara University. Drip water samples collected during 2017, 2018, and 2019 (n = 60) were analyzed on a Picarro L2130-i Isotopic Water Analyzer at Vanderbilt University. Rainwater samples were analyzed using a ThermoFinnigan Delta Plus XL isotope ratio mass spectrometer at the Stable Isotope Ratio Facility for Environmental Research (SIRFER) at the University of Utah. Further details on the

analytical approach are outlined in the Supplementary Materials (Text S1).  $\delta^{18}$ O and  $\delta^{2}$ H values are reported relative to Vienna Standard Mean Ocean Water (VSMOW).

### 3.1.2. Back trajectory analysis

We used the desktop version of the Hybrid Single Particle Lagrangian Integrated Trajectory Model (HYSPLIT) to evaluate potential moisture sources for precipitation in the LSC region (Stein et al., 2015). We used NCAR/NCEP reanalysis data to generate

back trajectories tracking air masses over the previous 72-h, beginning every 12 h at 2500 and 3500 m above sea level. Trajectories covered the period March 25, 2010 to October 20, 2015. To most closely match the weekly NADP CA76 rainwater isotope data set we used the rainfall record from the University of California Integrated Pest Management Program (UCIPM) weather station at Yreka, CA (6.4 miles west of NADP CA76) to identify rain days within each week. This resulted in a total of 128 generated trajectories for comparison with 140 weekly rainwater samples.

## 3.2. Stalagmite geochemistry

## 3.2.1. <sup>230</sup>Th/U dating

Both stalagmites were sliced along their growth axis. Fourteen subsamples from LSC3 and 8 subsamples from LSC2 were analyzed at the Berkeley Geochronology Center following procedures outlined in the Supplementary Text. Activity ratios and ages were calculated using the half-lives of Jaffey et al. (1971) for  $^{238}$ U, Holden (1989) for  $^{232}$ Th, and Cheng et al. (2013) for  $^{230}$ Th and  $^{234}$ U. Correction for U and Th from detritus was made assuming detritus with activity ratios of  $(^{232}$ Th/ $^{238}$ U) = 1.21  $\pm$  0.50,  $(^{230}$ Th/ $^{238}$ U) = 1.0  $\pm$  0.1, and  $(^{234}$ U/ $^{238}$ U) = 1.0  $\pm$  0.1. Ages are reported as years BP where present is 1950.

#### 3.2.2. Oxygen and carbon isotope analysis

Samples for stable isotope analysis ( $\delta^{18}$ O and  $\delta^{13}$ C) were milled along the growth axes of LSC3 and LSC2 from one of the cut faces of each stalagmite using a CM-2 micromill at Vanderbilt University at 100 µm spatial resolution. For LSC3, stable isotope samples were analyzed at this 100 µm sampling resolution during the slower growing portions of the stalagmite, while every third sample (effectively producing a 300 µm sampling resolution) was analyzed during the faster growing portions of the stalagmite. Alternating samples were analyzed throughout the LSC2 speleothem, resulting in ~200 µm spatial resolution. Sample powders were packed in weigh paper envelopes and sent to the Stable Isotope Biogeochemistry lab at Stanford University. There the samples were analyzed using a Thermo Finnigan Deltaplus XL coupled to a Gas-Bench. Typical precision of stable isotope measurements is < 0.2% for both oxygen and carbon. Final  $\delta^{18}$ O and  $\delta^{13}$ C values are expressed relative to the international standard V-PDB (Vienna PeeDee Belemnite).

## 3.2.3. Trace element analysis

Trace element concentrations were measured on thick sections along the growth axis of LSC3 using laser ablation ICP-MS using a Photon Machines Excimer laser coupled to a Thermo Finnigan iCapQ at Vanderbilt University. Analyses were conducted as line scans using a 20  $\times$  100  $\mu m$  rectangular slit at a scan speed of approximately 5  $\mu m/s$  at 20% laser power and a repetition rate of 10 Hz. Actual scan speeds varied for each line, and were back calculated by measuring line distance and elapsed scan time. The line scans followed a pre-ablation step that was conducted over the sample path at a scan speed of 10  $\mu m/s$  at 50% laser power at a repetition rate of 15 Hz. The multi-element synthetic glass standard NIST SRM 612 was used for elemental quantification using  $^{44}$ Ca. The synthetic pressed aragonite powder standard MACS3 was also analyzed at the beginning and end of each run. The data were processed using the lolite software package.

Trace element data are presented as ratios to calcium (mmolX/molCa). To facilitate visual comparisons of the records, each record was smoothed with a Gaussian kernel smoother using the locpoly function in the R package KernSmooth (Wand, 2019). The bandwidth for smoothing each record was chosen using the dpill

function in KernSmooth. To explore relationships among trace element to calcium ratios within each stalagmite, we conducted principal components analysis on log-transformed data using the FacoMineR package in R (Lê et al., 2008).

#### 4. Results

#### 4.1. Water isotopes

Our analysis of  $\delta^{18}$ O and  $\delta^{2}$ H in rain and drip waters demonstrates that all waters fall near the Global Meteoric Water Line. with similar calculated local meteoric water lines (Fig. 2A: Table S1). Samples of rainwater collected at NADP site CA76 show a wider range of variability than both the limited measurements of rainwater from Lake Shasta Caverns and the LSC drip water. This discrepancy may reflect a few factors. Rainwater samples from site CA76 are available for a longer period of time and are archived weekly, rather than monthly as the LSC rain samples were. Given the limited scope of the LSC rain sampling, our data likely do not reflect the full range of variation in precipitation  $\delta^{18}\mathrm{O}$  and  $\delta^{2}\mathrm{H}$ actually experienced at this site. It is also possible given the mountainous terrain of the region, that water vapor that reaches CA76 is more depleted of heavy isotopes than that which reaches LSC. Precipitation amount data from both sites between January 2015 and December 2015 indicate that rainfall occurs at the same time at these sites, but CA76 receives less rainfall than Lake Shasta (Figure S3).

Drip water from LSC falls along the same local meteoric water line as the LSC monthly integrated rainwater samples (Fig. 2A). The LSC drip water reaches values that are more depleted in <sup>18</sup>O and <sup>2</sup>H than the LSC rainwater, but spans a smaller isotopic range than the CA76 drip water. Drip water  $\delta^{18}$ O and  $\delta^{2}$ H displays the highest values during the late fall (November and December) and declines through the winter and early spring (Fig. 2B). Drip waters collected from all sites across the cave show similar values of  $\delta^{18}$ O and  $\delta^{2}$ H and similar seasonal patterns of variation, suggesting no clear trends with depth from the surface or location within the cave (Fig. 2B). For the amount of time that the CA76 and LSC drip water data overlap (December 2015–February 2017), the rainwater shows a similar pattern in seasonal  $\delta^{18}$ O and  $\delta^{2}$ H variability, with the drip water displaying approximately 1-month delay compared to rainwater (Fig. 2B). This delay is likely indicative of the time it takes for water to infiltrate the epikarst and reach the cave. This congruence provides confidence that, even though the CA76 rainwater isotope values are lower on the whole than LSC drip and rainwater, the seasonal patterns and overall and controls on variability are similar.

A similar pattern of variability in  $\delta^{18}O$  and  $\delta^{2}H$  is apparent during the entire period over which CA76 rainwater samples are available (March 2010–February 2017) (Figure S4). In general, CA-76 rainwater  $\delta^{18}O$  and  $\delta^{2}H$  are more negative during the winter and early spring and increase through the summer and autumn months (Table S1). This suggests that temperature may exert a control on the  $\delta^{18}O$  and  $\delta^{2}H$  signature of precipitation at this site over time. To assess this, we compared weekly average maximum, minimum and median temperatures from rain days recorded by the UCIPM weather station to the NADP CA-76 precipitation  $\delta^{18}O$  values. Spearman's rho "r" values were calculated for  $\delta^{18}O$  and weekly average minimum, median and maximum temperatures (0.40, 0.42 and 0.42 respectively with p < 0.001) indicating that temperature has a moderate control on the  $\delta^{18}O$  of precipitation that falls in Northern California in the modern day.

Results of NOAA HYSPLIT model backward trajectories reaching the CA-76 Montague site between March 2010 and October 2015 show that precipitation  $\delta^{18}$ O and deuterium excess are likely also

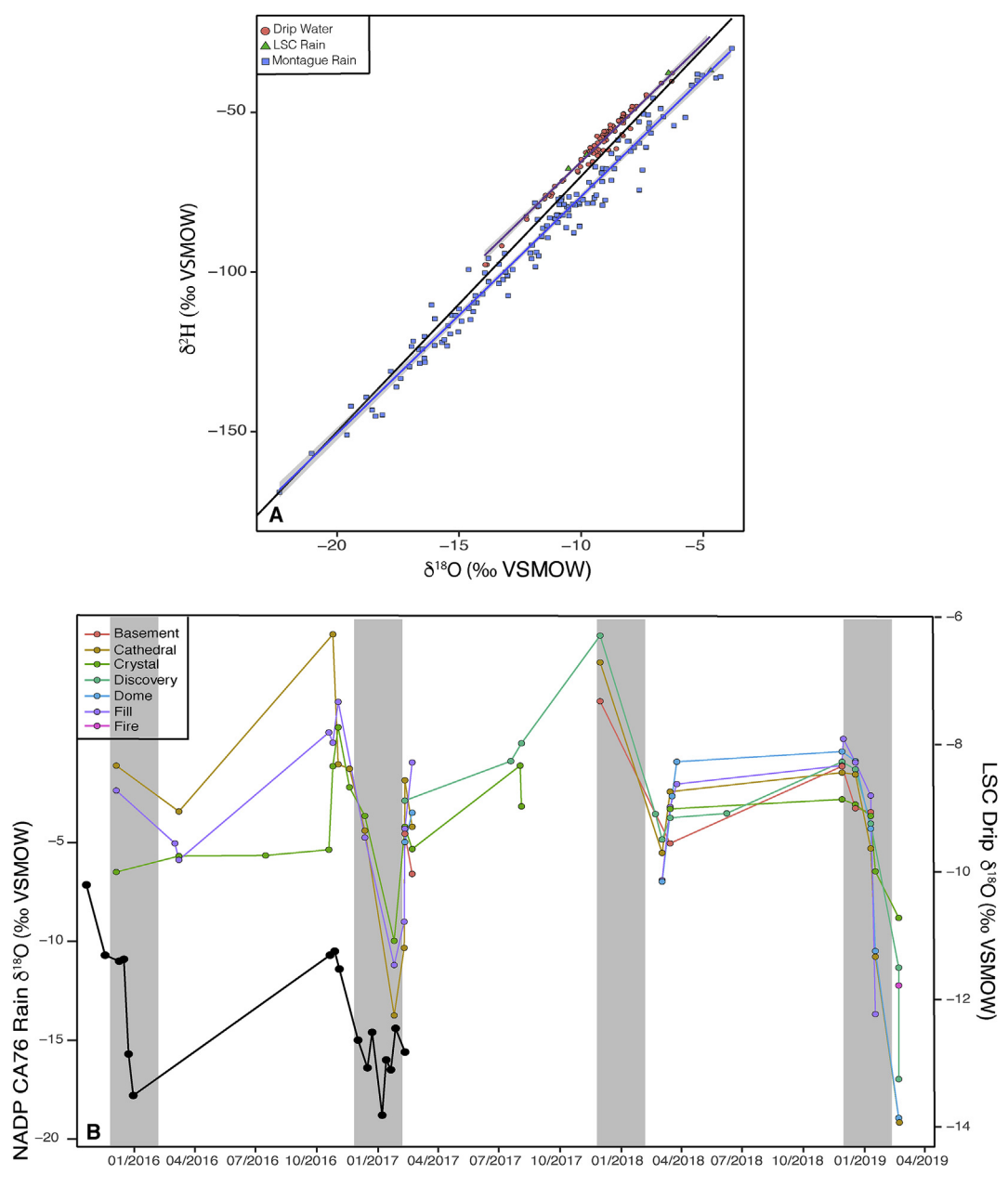


**Fig. 2.** A)  $\delta^{18}$ O vs.  $\delta^2$ H for rainwater collected from the NADP site CA76 in Montague, CA (squares), from the rainwater collector at LSC (triangles) and from cave drip water (circles). The global meteoric water line (black line) and linear regressions through the LSC rain and drip water data (purple line) and the CA76 rainwater data (blue line) including 95% confidence interval (gray shading) are also shown. B) Drip water  $\delta^{18}$ O from LSC drip sites with time (top) color coded by drip collection site (see Fig. 1 for site locations). Bottom black curve shows CA76 rainwater  $\delta^{18}$ O that temporally overlap with drip water collection (note different  $\delta^{18}$ O scale for drip and rain water). Gray bars highlight winter months (DJF). (For interpretation of the references to color in this figure legend, the reader is referred to the Web version of this article.)

related to moisture source. The deuterium excess, d-excess, defined as:

$$d-excess (\%) = \delta^2 H - 8 \times \delta^{18} O \tag{1}$$

where  $\delta^2 H$  and  $\delta^{18} O$  denote the deuterium and  $^{18} O$  abundance relative to VSMOW, is a second order isotope parameter that is specifically sensitive to the conditions during the evaporation of water from the ocean surface. Relative humidity is linearly correlated to d-excess, meaning when relative humidity is high, d-excess is low, and vice versa (Merlivat and Jouzel, 1979). The results of the 72-h back trajectory analysis at 2500 and 3500 m suggest that cool season storms originating in the subtropical Pacific (roughly below

 $40^{\circ}$ N) have lower d-excess, indicating humid conditions (blue circles, Fig. 3A and B). These back trajectories are also associated with more positive precipitation  $\delta^{18}$ O values (red circles; Fig. 3). Conversely, storms sourced in the North Pacific (roughly above  $40^{\circ}$ N) have higher d-excess (red circles; Fig. 3C and D), indicating lower humidity during evaporation, and generally more negative but also highly variable  $\delta^{18}$ O values (Fig. 3). Changes in temperature and humidity along ensemble trajectories for two representative rainfall events, one with back trajectories originating near the Aleutian Islands ( $\delta^{18}$ O of rainfall = -19.43%, d-excess = 13.4) and one with back trajectories originating near Hawai'i ( $\delta^{18}$ O of rainfall = -6.74%, d-excess = 5.1) are also shown in Figure S5. These show higher humidity along the transects from Hawai'i,

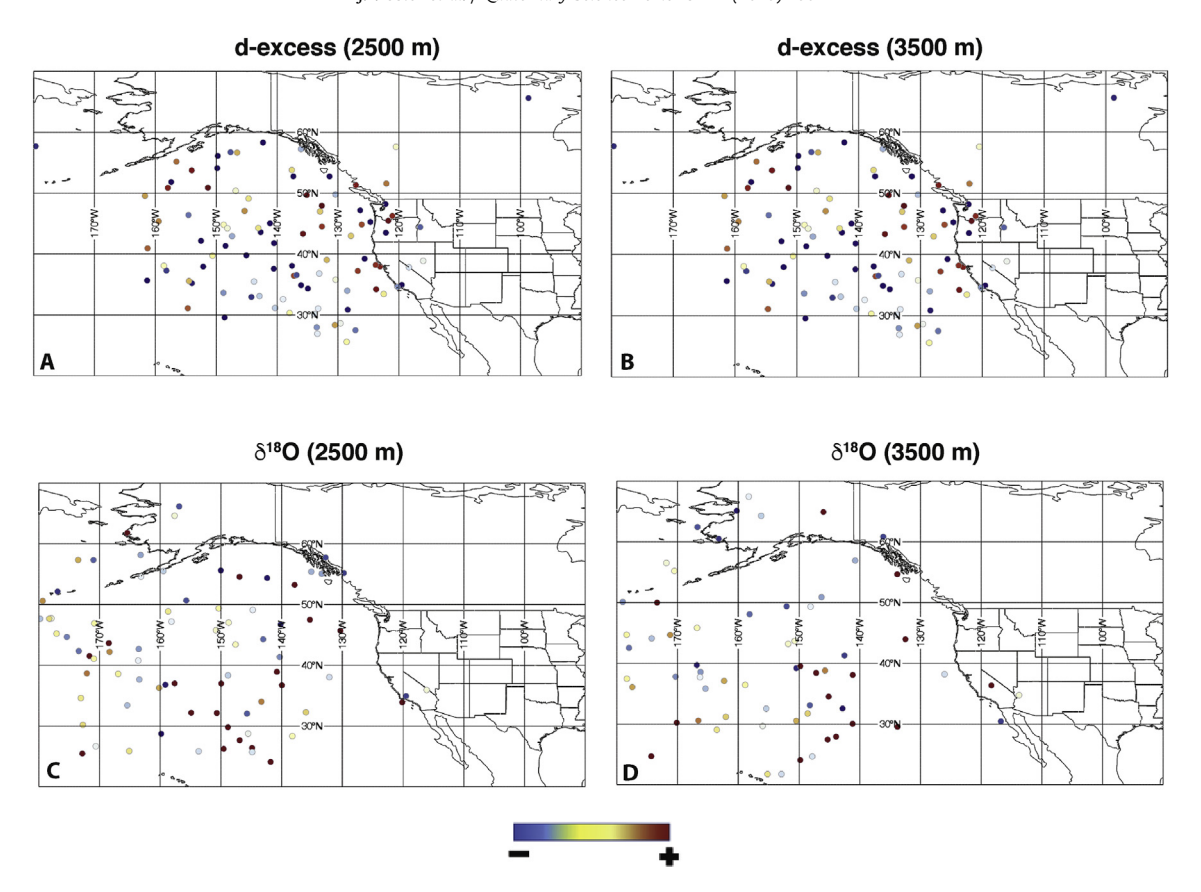


**Fig. 3.** Results of HYSPLIT back trajectory analyses. Circles show results of 72-h back trajectories for cool season (October–March) precipitation events beginning from the CA76 collection site at 2500 m a.s.l. (A, C) and 3500 m a.s.l. (B, D) Circles are color coded by d-excess (top panels) and  $\delta^{18}$ O (bottom panels) with higher values in warmer colors. (For interpretation of the references to color in this figure legend, the reader is referred to the Web version of this article.)

consistent with the lower d-excess for this rainfall event. Increasing humidity along the transects suggests moisture is acquired along the trajectories.

## 4.2. Stalagmite records

## 4.2.1. <sup>230</sup>Th/U dating

Analytical results and ages for stalagmites LSC2 and LSC3 are presented in Table 1. Both stalagmites are characterized by fairly low U concentrations (median ~90 ppb). Median uncertainty of the calculated  $^{230}$ Th/U ages is ~370 years (all errors  $2\sigma$ ). Dates from both stalagmites preserve stratigraphic order within analytical uncertainties. The stalagmites precipitated during the last glacial period and the beginning of the most recent deglaciation, LSC2 produced top and bottom ages of  $18,440 \pm 610$  and  $31,530 \pm 330$  yrs BP, respectively. LSC3 produced top and bottom ages of  $14,240 \pm 300$  and  $35,830 \pm 380$  yrs BP, respectively. The overlapping age ranges provide an opportunity to partially replicate stalagmite records from LSC during Marine Isotope Stage 2 (MIS2) including the LGM and Heinrich Stadial 2. As we are working with two partially overlapping stalagmites from the same cave, we used the algorithm iscam (intra-site correlation age modelling) in MATLAB to produce age-depth models for the geochemical proxies examined in each stalagmite (Fohlmeister, 2012) (Fig. 4). Iscam uses a Monte Carlo approach to find the best correlation between climate proxies from adjacent records during the overlapping interval and evaluates the correlation between these records, testing its significance against AR1 processes. Given that the proxies were sampled at two different time steps, we ran the iscam algorithm twice, once for stable isotopes using  $\delta^{18}O$  to correlate the two stalagmites, and once for trace elements using Sr/Ca to correlate the two stalagmites. Iscam found a correlation of r = 0.57 (all correlations tested for significance against AR1 processes) between the  $\delta^{18}\text{O}$  records of LSC3 and LSC2. For Sr/Ca, iscam found a correlation of r=0.46between the two stalagmites. Iscam found slightly lower, but comparable correlation coefficients for other trace elements (r = 0.39 for P/Ca and Ba/Ca). Stalagmite LSC3 grew more rapidly during the end of MIS3 (0.017 mm/yr between ~36,000 and ~29,000 yrs BP) and during Termination I (0.076 mm/yr between ~18,200 and 14,200 yrs BP) than during MIS2 (0.0027 mm/yr between ~29,000 and 18,200 yrs BP). By contrast, stalagmite LSC2 grew most rapidly during the LGM (0.028 mm/yr between ~22,700 and 21,200 yrs BP), with slower growth prior to the LGM (0.010 mm/vr between 22.700 and 27.600 vrs BP). Due to damage at the top and base of the LSC2 stalagmite, it was only possible to sample for stable isotope analysis between 15 and 100 mm from the top of the stalagmite. This produces a replicated record for LSC stable isotopes between ~21,200 and 27,600 yrs BP. For trace elements, which were analyzed on thin sections, we are able to produce an overlapping record for LSC stalagmites between ~18,000 and 24,000 yrs BP.

## 4.2.2. Stalagmite $\delta^{18}$ O and $\delta^{13}$ C

The spatial sampling resolution for the stable isotope analyses results in an average temporal resolution of ~26 years for the LSC3 speleothem. This resolution varies between sub-decadal for the most recent part of the deglaciation and parts of MIS3 to centennial or multi-centennial during the LGM. For the LSC2 stalagmite, the

Table 1 230Th/U analytical data and ages for stalagmites LSC2 and LSC3.

Sample Name	Depth from top (mm)	Sample Wt. (mg)	U (ppb)	<sup>232</sup> Th (ppb)	$(^{230}Th/^{232}Th)^{a}$	( <sup>232</sup> Th/ <sup>238</sup> U)	± (%) <sup>b</sup>	( <sup>230</sup> Th/ <sup>238</sup> U)	± (%)	( <sup>234</sup> U/ <sup>238</sup> U)	± (%)	Uncorrected Age (ka) <sup>c</sup>	Detritus- corrected Age (ka) <sup>d</sup>	Initial ( <sup>234</sup> U/ <sup>238</sup> U) <sup>e</sup>	Corrected Age (yr BP) <sup>f</sup>
LSC2-top	1	192.03	162.9	6.995	13.26	0.01381	0.15	0.1845	0.77	1.1167	0.54	19.77 ±0.10	18.50 ±0.61	1.1244 ±0.0065	18,440 ±610
LSC2-A	106	198.53	162.3	0.5581	225.5	0.00107	0.16	0.2554	0.56	1.0878	0.16	29.07 ±0.19	$28.98 \pm 0.20$	1.0954 ±0.0019	28,910 ±200
LSC2-C	95	196.65	101.3	4.413	16.77	0.01423	0.20	0.2403	0.58	1.1018	0.20	26.72 ±0.19	$25.56 \pm 0.63$	1.1107 ±0.0028	25,490 ±630
LSC2-E	60	196.41	89.40	0.6368	89.09	0.00224	0.06	0.2089	0.96	1.0998	0.23	22.89 ±0.25	$22.71 \pm 0.27$	1.1066 ±0.0027	22,640 ±270
LSC2-F	13	205.35	125.0	0.2711	270.8	0.00063	0.20	0.1913	0.38	1.0793	0.18	21.23 ±0.10	$21.17 \pm 0.10$	1.0842 ±0.0020	21,100 ±100
LSC2-G	30	163.13	104.6	0.2002	316.8	0.00052	0.20	0.1972	0.49	1.0918	0.24	21.67 ±0.13	21.62 ±0.13	1.0977 ±0.0027	21,550 ±130
LSC2-H	62	194.29	76.22	0.1211	397.6	0.00040	0.35	0.2056	0.50	1.0765	0.24	23.05 ±0.14	$23.02 \pm 0.14$	1.0817 ±0.0028	22,950 ±140
LSC2-bottom	125	154.06	139.3	0.9022	129.0	0.00198	0.18	0.2738	0.72	1.0797	0.49	31.99 ±0.16	31.59 ±0.33	1.0873 ±0.0058	31,530 ±330
LSC3-0.1 cm	1	198.60	102.5	0.9655	43.54	0.00272	0.12	0.1336	1.73	1.0697	0.20	14.80 ±0.28	14.30 ±0.30	1.0727 ±0.0022	14,240 ±300
LSC3-2 cm	20	193.42	101.5	0.6910	60.03	0.00205	0.11	0.1331	0.86	1.0577	0.61	14.92 ±0.17	$14.47 \pm 0.19$	1.0602 ±0.0067	14,400 ±190
LSC3-2.5 cm	25	197.46	98.38	0.1876	212.2	0.00054	0.12	0.1331	0.51	1.0653	0.16	14.54 ±0.08	14.49 ±0.087	1.0681 ±0.0018	14,430 ±90
LSC3-2.9 cm	29	186.78	59.51	0.2884	89.02	0.00108	0.08	0.1406	2.71	1.0737	0.36	15.78 ±0.46	$15.19 \pm 0.45$	1.0770 ±0.0041	15,130 ±450
LSC3-5.2 cm	52	197.56	58.41	0.8608	35.40	0.00419	0.54	0.1702	2.21	1.0724	0.22	19.27 ±0.47	$18.46 \pm 0.49$	1.0765 ±0.0025	18,390 ±490
LSC3-5.8 cm	58	197.63	84.25	0.4848	88.86	0.00178	0.08	0.1680	0.77	1.0837	0.18	18.33 ±0.16	$18.19 \pm 0.17$	1.0883 ±0.0020	18,120 ±170
LSC3-6.2 cm	62	199.63	85.58	2.742	20.21	0.01041	0.54	0.2127	0.60	1.0724	0.19	24.05 ±0.17	$23.18 \pm 0.48$	1.0779 ±0.0024	23,110 ±480
LSC3-7.6 cm	76	198.30	52.53	0.7325	53.31	0.00387	0.11	0.2421	1.31	1.0750	0.84	28.20 ±0.51	$27.42 \pm 0.52$	1.0812 ±0.0097	27,350 ±520
LSC3-8.1 cm	81	187.40	49.93	0.4225	92.77	0.00210	0.09	0.2562	1.06	1.0835	0.24	29.80 ±0.37	$29.14 \pm 0.38$	1.0908 ±0.0028	29,070 ±380
LSC3-10.6 cm	106	194.76	55.90	0.6288	76.61	0.00305	0.06	0.2809	1.38	1.1025	0.29	$32.32 \pm 0.53$	$31.68 \pm 0.54$	1.1123 ±0.0034	31,610 ±540
LSC3-12 cm	120	197.70	78.21	11.56	6.240	0.04842	0.11	0.3029	0.62	1.0736	0.24	$36.00 \pm 0.29$	$31.89 \pm 2.17$	1.0839 ±0.0056	31,820 ±2170
LSC3-12.9 cm	129	195.62	99.28	0.4284	195.4	0.00108	0.23	0.2747	0.91	1.0625	0.25	$32.76 \pm 0.36$	$32.43 \pm 0.36$	1.0685 ±0.0029	32,360 ±360
LSC3-15 cm	150	197.99	77.50	0.4438	149.2	0.00166	0.22	0.2784	0.77	1.0597	0.52	33.46 ±0.37	$32.99 \pm 0.37$	1.0656 ±0.0060	32,930 ±370
LSC3-17.3 cm	173	197.38	93.23	0.4268	202.4	0.00115	0.22	0.3020	0.83	1.0706	0.24	$36.23 \pm 0.37$	35.90 ±0.37	$1.0782 \pm 0.0028$	35,830 ±370

<sup>&</sup>lt;sup>a</sup> All isotope ratios are activity ratios. Decay constants are those of Jaffey et al. (1971) for <sup>238</sup>U and Cheng et al. (2013) for <sup>230</sup>Th and <sup>234</sup>U.

<sup>&</sup>lt;sup>b</sup> Uncertainties are given at two standard deviations.

between the two standard activations.

C Uncorrected ages are calculated from measured ratios.

Detritus-corrected ages were corrected for initial  $^{230}$ Th,  $^{234}$ U, and  $^{238}$ U using  $^{232}$ Th/ $^{238}$ U) = 1.21  $\pm$  0.50,  $^{230}$ Th/ $^{238}$ U) = 1.0  $\pm$  0.1, and  $^{234}$ U/ $^{238}$ U) = 1.0  $\pm$  0.1.

Initial  $^{234}$ U/ $^{238}$ U) is back-calculated from the measured ratio and the detritus-corrected  $^{230}$ Th age.

f Corrected age (yr BP) stands for years before present, where present is defined as 1950 A.D., rounded to nearest decade.

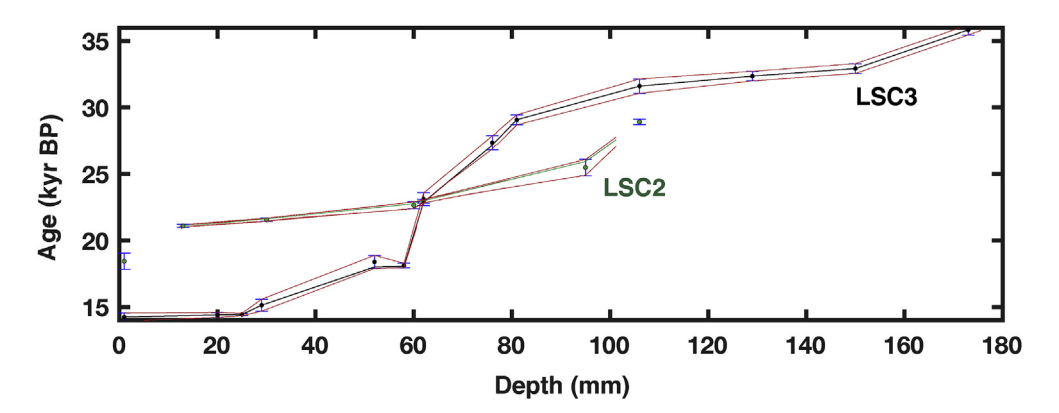


Fig. 4. Age models for stalagmites LSC3 (black) and LSC2 (green) with associated 95% confidence limits (red) generated with iscam for the stable isotope records (Fohlmeister, 2012). Ages are shown with  $2\sigma$  errors. Due to sample damage, proxy information is not available for the youngest or oldest part of LSC2, so the age model does not extend to these parts of the stalagmite, though these ages are included in the modeling algorithm. (For interpretation of the references to color in this figure legend, the reader is referred to the Web version of this article.)

spatial sampling resolution produces an average temporal resolution of 35 years (varying between ~4 and 160 years). For LSC3,  $\delta^{18}$ O values range from -8.04 to -10.44% (all values reported relative to VPDB). For LSC2,  $\delta^{18}$ O values range from -8.38 to -9.72%. LSC3  $\delta^{18}$ O values for the period of time overlapping with the LSC2 record cover a similar range (-8.04 to -9.6%). LSC3  $\delta^{13}$ C values range from -2.35 to -7.38%. LSC2  $\delta^{13}$ C values show a similar overall range (-2.76 to -6.98%). Overall, the  $\delta^{18}$ O records between the two stalagmites reproduce well, and iscam produced a correlation coefficient of 0.57 between the two records. However, the faster growing stalagmite during any one interval displays more overall variability (Fig. 5). The same is true to greater degree when comparing the  $\delta^{13}$ C records between the two stalagmites. For example, the LSC2  $\delta^{18}$ O and  $\delta^{13}$ C records display larger and more rapid variations across Heinrich Stadial 2 (HS2) and during the height of the glacial period than the LSC3 record, while the LSC3 stalagmite displays larger and more rapid variations prior to HS2. The direction of change within both records is similar during their period of overlap with the exception of the oldest portion of the LSC2  $\delta^{13}$ C record. Between 25,500 and 27,600 yrs BP, growth of stalagmite LSC2 is slower and  $\delta^{13}$ C values are more elevated than during the peak glacial part of this record.

For both stalagmites,  $\delta^{18}{\rm O}$  and  $\delta^{13}{\rm C}$  values display distinct multimillennial trends, overprinted by multi-centennial to millennial scale abrupt changes (Fig. 5). The  $\delta^{18}{\rm O}$  records display overall less variability and fewer abrupt changes than the  $\delta^{13}{\rm C}$  records. In the longer LSC3 record,  $\delta^{18}{\rm O}$  values are at their highest during MIS2 through the LGM, with lower values during the interglacial MIS3 and the most recent deglaciation. LSC3  $\delta^{18}{\rm O}$  values decrease sharply at the beginning of Heinrich Stadial 1 (HS1). LSC3  $\delta^{13}{\rm C}$  values are characterized by millennial-scale oscillations, in particular during the MIS3 portion of the record. Although these oscillations are less pronounced during the MIS2 portion of the record, the faster growing LSC2 stalagmites suggests that abrupt centennial-millennial scale oscillations may still be occurring, but the slower growing LSC3 stalagmite does not capture them in this interval.

#### 4.2.3. Stalagmite trace element ratios

Relative abundances of trace elements display centennial to millennial scale variations across the measured interval of both stalagmites. Smoothed time series for Mg/Ca, P/Ca, and Sr/Ca are shown in Fig. 5 compared to the stable isotope records, and raw data with smoothers are shown in Figure S6. As LSC2 is generally faster growing and thus of higher temporal resolution than LSC3

across the interval in which the trace element data overlap, the optimum smoothing bandwidth for LSC2 produces a record that displays higher frequency variability. Similar to the stable isotope records, LSC2 displays larger and more abrupt variations in Sr/Ca and P/Ca than LSC3 during the period of overlap, the full glacial. Mg/Ca shows a similar overall range between the two records. In general, the centennial and multi-centennial variations in Sr/Ca. P/ Ca. and Mg/Ca are similar between the two stalagmites. However. there are intervals that display exceptions to this. The Sr/Ca record for LSC2 displays a peak near 22.500 yrs BP that is not apparent in the LSC3 record and shows more elevated values during HS2. Additionally, while both stalagmites show lower Sr/Ca between ~18,000 and 19,500 yrs BP, the LSC2 record shows a sharp peak in the middle of this interval that the LSC3 record does not. The Mg/Ca records for the two stalagmites also show different behavior between and ~20,800 and 22,400 yrs BP when LSC2 indicates a decrease followed by an abrupt increase in Mg/Ca, while LSC3 shows a more gradual decline through the interval. For both stalagmites, Mg/Ca and  $\delta^{13}$ C show similar changes during MIS2 (Fig. 5).

The principal components analysis of both stalagmites produces similar results (Fig. S7). Notably, Sr/Ca and Ba/Ca cluster together for both stalagmites, suggesting that these ratios are controlled by changes in prior carbonate precipitation (PCP) along the seepage water flow path (e.g. Tremaine and Froelich, 2013). The ratios of Zn, Cu, U, and P to Ca are closely related to each other in both stalagmites and may reflect input of these elements from the soil zone above the cave (Hartland et al., 2012; Oster et al., 2017). For LSC3 and LSC2, Mg/Ca plots in between this group of more soil-derived elements (P, Cu, Zn) and the PCP-controlled Sr/Ca and Ba/Ca. This suggests that Mg/Ca is not only controlled by PCP, but likely responds to some combination of PCP and inputs from the soil or host rock dissolution.

#### 5. Discussion

#### 5.1. Stalagmite proxy interpretations

## 5.1.1. $\delta^{18}$ O and $\delta^{13}$ C

Analysis of drip water  $\delta^{18}$ O and  $\delta^{2}$ H at LSC demonstrates that drip water isotope values fall along a local meteoric water line (Fig. 2A), suggesting minimal modification of drip waters by evaporation or other epikarst processes. Drip water  $\delta^{18}$ O analyzed at multiple sites within the cave also shows similar variability. Furthermore, for the period of time over which LSC drip water and measurements of CA76 rainfall data overlap, they show similar

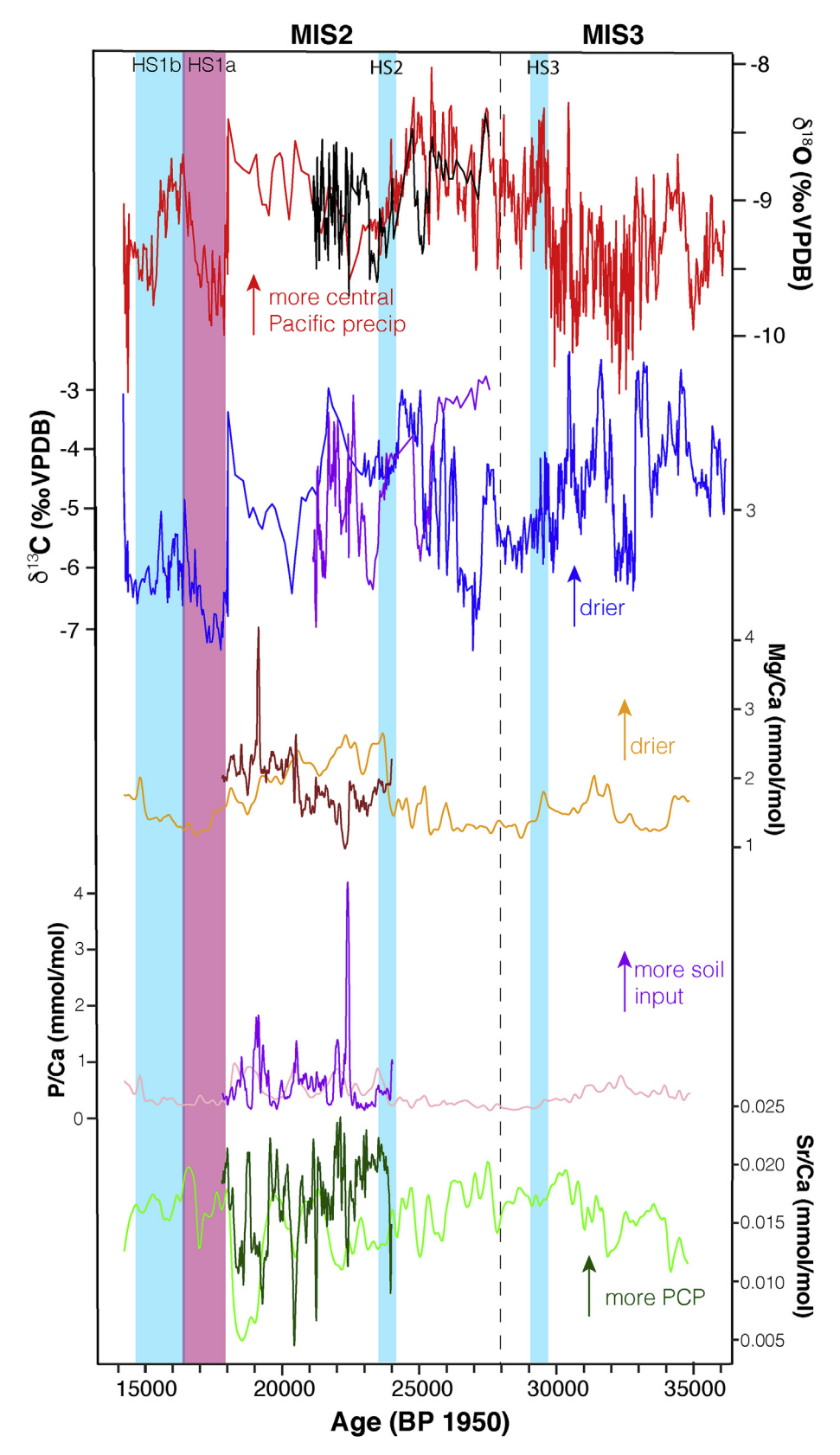


Fig. 5. Comparison of LSC time series. From top to bottom:  $\delta^{18}$ O for LSC3 (red) and LSC2 (black);  $\delta^{13}$ C for LSC3 (blue) and LSC2 (purple); Mg/Ca for LSC3 (orange) and LSC2 (brown); P/Ca for LSC3 (pink) and LSC2 (purple), and Sr/Ca for LSC3 (light green) and LSC2 (dark green). Heinrich events are shown in blue, with timing of events after Cheng et al. (2016). The relative timing of the HS1a and HS1b is also shown. Dashed line separates MIS2 and MIS3. (For interpretation of the references to color in this figure legend, the reader is referred to the Web version of this article.)

isotopic variability, with  $\delta^{18}$ O values decreasing from the late fall through the winter and rising again into the spring (Fig. 2). These observations suggest that LSC drip water  $\delta^{18}$ O should reflect the local pattern of rainwater  $\delta^{18}$ O variability and that this pattern is preserved in drip water  $\delta^{18}$ O throughout the cave.

Comparison of the CA76 rainwater  $\delta^{18}$ O and  $\delta^{2}$ H values with measurements of air temperature and the HYSPLIT back-trajectory analysis suggests that Northern California rainwater isotopic values likely respond to both temperature and moisture origin and transport history. This relationship is supported by the moderate correlation between precipitation  $\delta^{18}$ O and air temperature during precipitation events ( $r_s = 0.40-0.42$ , p < 0.001). The HYSPLIT results (Fig. 3) show that a cluster of rainfall events associated with the most positive rainwater  $\delta^{18}$ O and the lowest d-excess values originated in the central Pacific (roughly below 40°N). A high  $\delta^{18}$ O and low d-excess, reflecting more humid conditions at the time of evaporation, as well as the origination along a trajectory between Hawai'i and the west coast of North America suggest these rainfall events may be associated with Atmospheric River (AR) storms, which tend to be warm and wet for California winter precipitation events (Dettinger, 2004). For example, one AR storm passed over the cave between late November and early December of 2012 (November 27- December 3). Weekly integrated precipitation collected from site CA-76 between November 27 and December 4, 2012 recorded a  $\delta^{18}$ O value of -4.01%. Comparatively, during the week prior. November 20-27, 2012, the  $\delta^{18}$ O of weekly integrated precipitation was -10.35%. The  $\delta^{18}$ O of weekly integrated precipitation collected between December 4–11, 2012, the week following the AR event, had a  $\delta^{18}$ O value of -13.09%.

Previous rainfall, cave drip water, and speleothem studies from southern Oregon attributed water and speleothem  $\delta^{18}$ O variability to changes in local atmospheric temperature at the time of precipitation (Ersek et al., 2010, 2012). Similar work from central California, south of LSC, found that both temperature and moisture source can influence rainwater, and therefore speleothem  $\delta^{18}O$ (Oster et al., 2012, 2015b; 2017). An analysis of extreme precipitation events, including AR events in California over ten years found wide variation in the  $\delta^{18}$ O of precipitation during these events that reflect myriad drivers (McCabe-Glynn et al., 2016). However, observations of modern event-scale precipitation  $\delta^{18}$ O at sites along the US west coast (Berkelhammer et al., 2012; Vachon et al., 2010) suggest that seasonal and interannual variability in precipitation  $\delta^{18}$ O is due to varying proportions of moisture from subtropical versus mid-latitude and north Pacific-derived sources. In the context of this work and our analysis of precipitation at CA-76, it is likely that both air temperature and the proportion of moisture from the central versus northern North Pacific influence the  $\delta^{18}$ O of rainwater and cave drip waters during the period of time covered by the LSC speleothem records.

Speleothem  $\delta^{18}$ O may be influenced by non-equilibrium isotope fractionation due to rapid degassing and calcite precipitation (e.g. Mickler et al., 2004). The low to moderate correlations between  $\delta^{18}$ O and  $\delta^{13}$ C for the LSC speleothems (r = 0.25 for LSC3, r = 0.42 for LSC2, neither with significant p values) indicates that kinetic effects during calcite precipitation are not the dominant influence on these records. More importantly, the generally good reproducibility within age uncertainty of variations in speleothem  $\delta^{18}$ O (r = 0.57) for these two stalagmites provides evidence that they are each recording environmental signals (e.g. Dorale and Liu, 2009). Up to 90% of rainfall in Northern California occurs during the cool season (Oct.-Mar.), and this seasonality is also reflected in drip water behavior in the cave (D. Mundt Pers. Comm.). Thus, we anticipate that the cool season is the primary season of speleothem growth within LSC and that proxy signals are likely biased toward cool season climates.

Pollen and plant macrofossil data from the Siskiyou Mountains provide evidence that there is no significant presence of C4 flora during the last glacial and deglaciation near LSC (Briles et al., 2005), so changes in plant community structure should not influence speleothem  $\delta^{13}$ C on the timescales recorded by the LSC stalagmites. Cave monitoring studies and speleothem records from similar semi-arid, mountainous regions in western North America including coastal Oregon (Ersek et al., 2012), the Sierra Nevada foothills (Oster et al., 2012), California Coast Range (Oster et al., 2017), and the Great Basin (Steponaitis et al., 2015) suggest that carbon isotope signatures in cave drip waters and speleothems reflect changes in water supply via their influence on soil processes and degassing in the epikarst and within the cave itself. Both of these processes tend to shift speleothem  $\delta^{13}$ C in the same direction in response to changes in water availability above the cave, with increased rainfall leading to increased soil respiration and decreased drip water degassing, causing a negative shift in speleothem  $\delta^{13}$ C, and vice versa (e.g. Ersek et al., 2012; Oster et al., 2015b, 2017). It has also been suggested that speleothem  $\delta^{13}$ C responds to changes in atmospheric pCO2 through its influence on the fractionation of carbon isotopes during C3 photosynthesis (Breecker, 2017). This effect would contribute a gradual ~0.8% decrease in LSC  $\delta^{13}$ C between ~20,000 yrs BP and the end of the record at ~14,000 yrs BP as atmospheric pCO2 rose following the LGM (Breecker, 2017). This may explain part of the >2% shift we observe in the LSC3 record coming out of the LGM. However, the changes in this record are generally abrupt and not unidirectional. and thus more likely reflect rapid regional or local changes in climate rather than gradual, global changes in pCO<sub>2</sub>

Variations in LSC  $\delta^{18}$ O across the time period covered by these stalagmites suggest centennial to multi-millennial scale changes in precipitation moisture source and temperature that were concurrent with global climate events (Fig. 5). The  $\delta^{18}$ O of LSC3 is generally more negative during the MIS3 and deglacial portions of the record, and more positive between Heinrich Event 3 (HS3) and the onset of Heinrich Event 1 (HS1). Regionally, clumped isotope measurements from shore zone tufas deposited in glacial Lake Chewaucan approximately 250 km to the northeast of LSC suggest a temperature depression of 7  $\pm$  3 °C during the full glacial compared to modern conditions, with tufas dating to 14 ka indicating a range of temperatures between the modern and full glacial estimates (Hudson et al., 2017). Colder air temperatures should lead to more negative precipitation, and therefore more negative speleothem  $\delta^{18}$ O. Thus, the generally higher values for  $\delta^{18}$ O during the full glacial portion of the record compared to the MIS 3 and deglacial parts of the record argue against temperature being the dominant control on speleothem  $\delta^{18}$ O via its influence on water  $\delta^{18}$ O. However, using the cave-specific calcite-water temperature relationship developed by Tremaine et al. (2011), a 7 °C decrease in average annual temperature would result in an ~1.2% increase in speleothem calcite  $\delta^{18}$ O due to the influence of temperature on isotopic fractionation during the precipitation of calcite within the cave. This magnitude of change is comparable to what is observed in the LSC3 record between the LGM and the onset of HS1a, and so temperature effects on in-cave calcite precipitation cannot be entirely ruled out as an influence on the LSC3  $\delta^{18}$ O. However, the abrupt nature of the centennial to millennial-scale shifts in  $\delta^{18}{\rm O}$  that occur throughout the record indicate that they likely cannot be explained by glacial-interglacial variations in temperature but rather may reflect shifts between predominantly North Pacific or Central Pacific moisture sources and trajectories (Fig. 5).

## 5.1.2. Trace elements

A principal components analysis of trace element to calcium ratios produces very similar results for LSC2 and LSC3 (Fig. S7).

Principal Component 1 (PC 1) explains 25–28% of the variability in the datasets and is most likely related to overall concentration of trace elements within the stalagmite calcite. PC2 explains 21–23% of the variations in the datasets and primarily separates Sr/Ca and Ba/Ca from the other ratios, mainly P/Ca and U/Ca. In LSC2 this group also includes Zn/Ca and Cu/Ca. The Mg/Ca ratios plot in between these groups for both stalagmites, but are closely associated with Zn/Ca and Cu/Ca for LSC3. In stalagmites, Sr/Ca and Ba/Ca often show similar behavior related to prior carbonate precipitation (PCP), which refers to calcite, and in some cases aragonite, precipitation within the epikarst or on cave ceilings upflow from the stalagmite growth site (Fairchild et al., 2000). On the other hand, elements such as P, Zn, and Cu in cave systems are often associated with soil-derived organics in drip water and can be related to pulses of infiltration that also transport particulate organic matter and colloids into the cave (Borsato et al., 2007; Hartland et al., 2012; Rutlidge et al., 2014). A comparison of Mg/Ca with both P/Ca, which reflects inputs from the soil, and Sr/Ca which responds to PCP, could illuminate the most important drivers for determining stalagmite Mg/Ca through time. For the LSC3 stalagmite, Mg/Ca shows small amplitude, multi-centennial variations that are similar in timing to comparably larger variations in Sr/Ca. However, larger, and more long-lasting changes in Mg/Ca, such as the elevated values between ~29,000 and ~32,200 yrs BP and between HS1 and HS2, align with similar increases in P/Ca. Likewise, complex behavior is apparent in the LSC2 record, with Mg/Ca displaying similarities with both Sr/Ca and P/Ca at different times.

Broadly, stalagmite Mg/Ca often exhibits behavior that is similar to Sr/Ca and Ba/Ca, and the correlation between Mg/Ca and Sr/Ca has been used to diagnose PCP in karst systems and relate this to paleoenvironmental change (Sinclair et al., 2012; Tremaine and Froelich, 2013). However, stalagmite Mg has also been linked to the influx of soil particulates to cave systems (Belli et al., 2017). Previous studies of California speleothems have demonstrated that stalagmite Mg/Ca in these cave systems can also respond to other drivers, including variations in the dissolution of dolomite or other Mg-rich phases within the host rock (Oster et al., 2014, 2017). In such cases, Mg does not follow the single source rule outlined by Tremaine and Froelich (2013) and cannot act as an indicator of PCP alone. The McCloud limestone that hosts LSC consists mainly of calcarenite that is composed of varying degrees of crinoid fragments which are composed of high-Mg calcite and also displays variable degrees of dolomitization (Demirmen and Harbaugh, 1965). Thus, it is possible that differential dissolution of high-Mg calcite, which tends to react more easily than low-Mg calcite (Busenberg and Plummer, 1989) or dolomite, which reacts more slowly than calcite (Chou et al., 1989) may be contributing Mg to the LSC seepage water and speleothems. The intermediate association of Mg/Ca with both rock derived elements (Sr. Ba) and soil derived elements (P, Zn, Cu) as well as the complex relationships of Mg/Ca with Sr/Ca and P/Ca through time further suggests that stalagmite Mg/Ca likely reflects a combination of soil-derived and bedrock derived Mg that is influenced by PCP.

Like Mg/Ca and as discussed previously, stalagmite  $\delta^{13}$ C can also be subject to numerous complex controls (e.g. Fohlmeister et al., 2020). Mg/Ca and  $\delta^{13}$ C displays similar variations throughout the LSC3 record, with decreases in Mg/Ca associated with decreased  $\delta^{13}$ C and vice versa. For example, the overall rise of Mg/Ca in LSC3 at the onset of MIS2 and decline to the onset of HS1 is similar to  $\delta^{13}$ C, suggesting similar broad scale controls on the two records. As with Mg/Ca,  $\delta^{13}$ C displays similar centennial to multi-centennial scale variations to Sr/Ca, especially during MIS3 and HS1. This indicates that PCP may be responsible for small and short-lived changes in stalagmite Mg/Ca and  $\delta^{13}$ C, but that the broader, millennial-scale changes are likely due to a combination of soil processes and/or

water-rock interactions. The P/Ca ratio of both stalagmites is elevated throughout most of the full glacial period, between and ~18,000 and 23,000 years BP. The increased P/Ca during glacial conditions suggests a higher influx of soil-derived organic material to the cave at this time, likely bringing variable amounts of Mg, leading to an imprint of soil Mg on top of the water-rock interaction and PCP signals. Enhanced stalagmite P/Ca has been interpreted to reflect periods of elevated recharge into cave systems (e.g. Oster et al., 2017). However, the overall high  $\delta^{13}$ C during MIS2, compared with the deglacial interval and the highly variable MIS3, argues against wetter conditions during this interval that would suppress degassing of CO<sub>2</sub> in the epikarst and promote soil respiration. Rather, we hypothesize that the cold, potentially dry conditions of MIS2 and the full glacial promoted soil erosion during this time, leading to elevated P/Ca in the drip water and speleothem and periods of increased soil-derived Mg/Ca. Likewise, Sr/Ca in both stalagmites suggests intervals of enhanced PCP, especially during the LGM between ~20,000 and 22,000 yrs BP.

#### 5.1.3. Climate interpretations from the LSC proxy records

Taken together, the stable isotope and trace element ratio records from LSC3 and LSC2 paint a nuanced picture of climate response in northern California between MIS3 and the last deglaciation. During MIS3, centennial to millennial scale shifts to more negative  $\delta^{18}$ O occur coincident with Dansgaard-Oeschger (D-O) events 3 through 7 as noted in the NGRIP Greenland ice core record (Wolff et al., 2010). These shifts to more negative  $\delta^{18}$ O are also associated with more negative  $\delta^{13}$ C in the LSC3 record (Figs. 5 and 6), suggesting that D-O interstadials are associated with wetter conditions at LSC, with increased rainfall sourced from the northern Pacific. The Mg/Ca record of stalagmite LSC3 also shows low values during D-O interstadials 3-6 (Fig. 5), in support of wetter conditions. The decreases in  $\delta^{13}$ C are associated with minor decreases in Sr/Ca during D-O interstadials 3, 4, the end of 5, and the beginning of 6. This suggests changes in PCP are occurring, but that PCP is not the dominant control on  $\delta^{13}C$  and also indicates that cave air ventilation may have played an important role in modulated PCP in addition to water supply, as seen in caves in the central Sierra Nevada (Oster et al., 2012).

By comparison, the HS3 interval is coeval with an abrupt shift to more positive  $\delta^{18}{\rm O}$  in LSC3 and moderate shifts to more positive  $\delta^{13}{\rm C}$ , higher Mg/Ca, and overall elevated Sr/Ca indicating potentially more subtropical-sourced storms associated with the Heinrich Event as well as somewhat drier conditions and high PCP. Heinrich Event 2, by contrast is not associated with a positive shift  $\delta^{18}{\rm O}$ , but is coeval with an interval of relatively decreased  $\delta^{13}{\rm C}$  in LSC3 and decreasing  $\delta^{13}{\rm C}$  in LSC2. Mg/Ca and P/Ca are elevated, indicating more soil inputs. These observations indicate that D-O interstadials were associated with increased moisture in northern California with more complex signals during Heinrich Events 2 and 3 that may be consistent with moderate, short-lived drying.

Comparison of stable isotopes and trace element ratios suggests that MIS2 was dry compared to the MIS3 and deglacial parts of the LSC record. This is signified by higher  $\delta^{13}\mathrm{C}$  and Mg/Ca values in LSC3 and in the part of LSC2 that approaches the period of the LGM. LSC2 does indicate there was more variability than was captured by the slower growing LSC3 stalagmite. However, the higher Mg/Ca values in LSC2 between ~18,000 and 21,000 years BP lend further support to the interpretation of drier conditions during the LGM. The elevated P/Ca values may indicate enhanced soil erosion above the cave due to cold, dry conditions with reduced vegetation. The overall higher  $\delta^{18}\mathrm{O}$  during MIS2 may reflect colder average annual temperatures that influence isotopic fractionation during calcite precipitation within the cave. However, these elevated values may also suggest an increased proportion of moisture reaching the cave

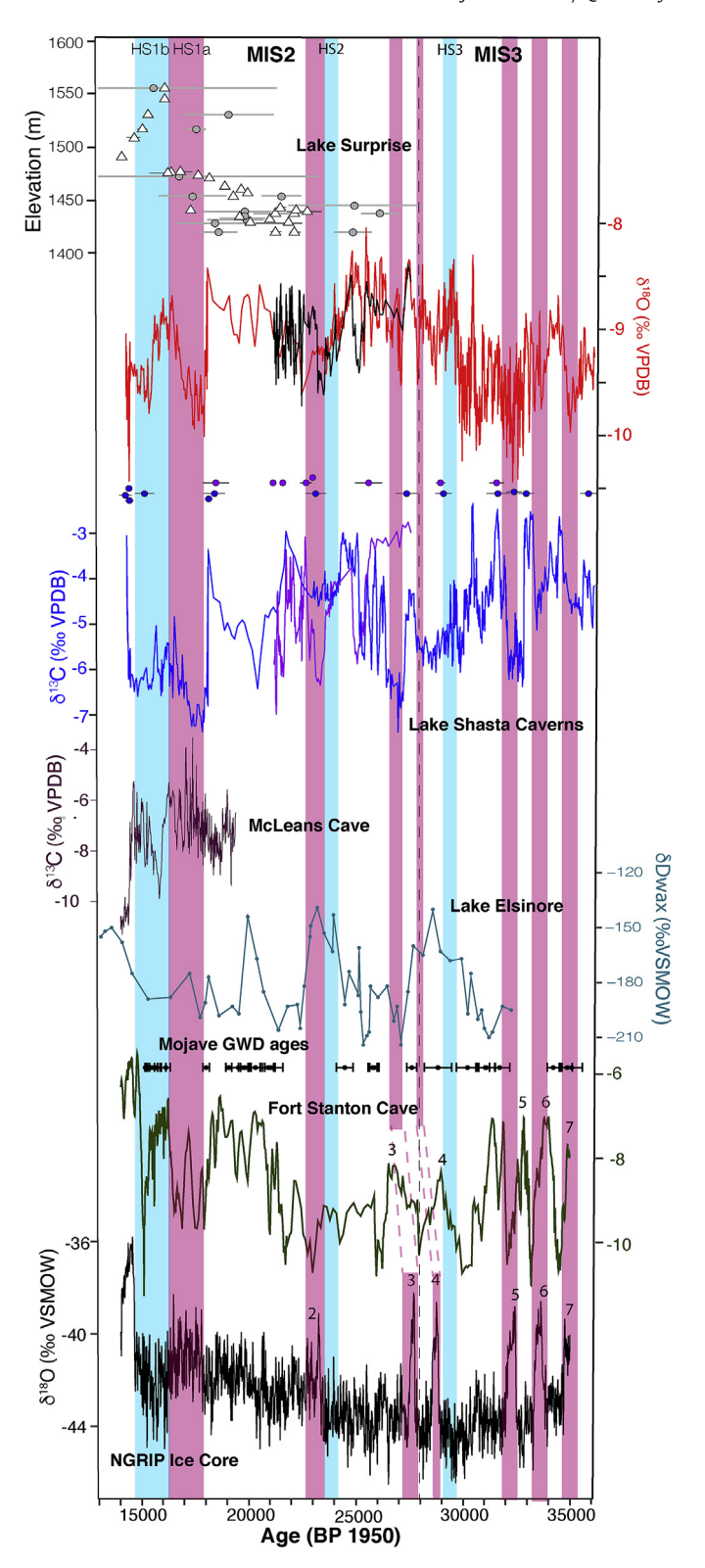


**Fig. 6.** From top to bottom: Lake Surprise, CA lake level elevation, circles: U-series ages uncertainties (Ibarra et al., 2014), triangles  $^{14}\text{C}$  ages (Egger et al., 2018; Ibarra et al., 2014) all uncertainties  $2\sigma$ ; LSC  $\delta^{18}\text{O}$  for LSC3 (red) and LSC2 (black); LSC  $\delta^{13}\text{C}$  for LSC3 (blue) and LSC2 (purple), U-series ages and  $2\sigma$  uncertainties for LSC stalagmites are shown above the  $\delta^{13}\text{C}$  curves; McLean's Cave  $\delta^{13}\text{C}$  (Oster et al., 2015b); Lake Elsinore leaf wax δD (Feakins et al., 2019); Ages and 2  $\sigma$  uncertainties for Mojave groundwater deposits (black) (Springer et al., 2015); Fort Stanton Cave  $\delta^{18}\text{O}$  (green) (Asmerom et al., 2010); and NGRIP Greenland Ice Core  $\delta^{18}\text{O}$  (black) (Svensson et al., 2008). D-O interstadials are numbered for NGRIP and Fort Stanton according to original publications. Heinrich Events are noted as in Fig. 5. Pink bars highlight the

from the Central rather than the Northern Pacific. This increase may indicate increased subtropical rainfall from atmospheric rivers, which has been suggested for this region during LGM based on climate model simulations (Lora et al., 2017). Climate models generally place the boundary for wetter versus drier than modern conditions at the LGM very close to the latitude of LSC along the western coast of North America (Oster et al., 2015a; Lora et al., 2017), with drier conditions to the north and wetter conditions to the south. Thus, it is plausible that LSC would sit on the northern boundary of the zone of wetter LGM conditions and experience an increase in the proportion of Central Pacific precipitation relative to North Pacific derived precipitation while not experiencing an overall increase in precipitation.

Following the LGM, the LSC3 stalagmite displays decreases in  $\delta^{18}$ O,  $\delta^{13}$ C, and Mg/Ca that would be consistent with enhanced delivery of North Pacific sourced moisture to the cave and wetter conditions. These changes are especially pronounced during the first part of Heinrich Stadial 1, which is coincident with the "Big Dry" event noted in some southwestern U.S. pluvial lake records (Broecker et al., 2009) more recently referred to as "HS1a" (18,000-16,100 years BP) (Hudson et al., 2019). Although the proxies show increasing values after this interval,  $\delta^{13}$ C, and Mg/Ca remain lower than their glacial values, suggesting that conditions remained wetter throughout HS1 compared to the LGM. As with MIS3, small scale changes in Sr/Ca align with  $\delta^{13}$ C during HS1 suggesting that PCP is only one influence on  $\delta^{13}$ C. This is consistent with a recent synthesis of global speleothem  $\delta^{13}$ C that found vegetation and soil respiration are important influences on  $\delta^{13}$ C. in addition to PCP (Fohlmeister et al., 2020).

#### 5.2. Regional climate relationships

The LSC record provides a unique opportunity to investigate hydroclimate in western North America across an interval of dynamic change. Its location near the transition between the Southwest and the Pacific Northwest, which exhibit different hydroclimatic behavior in response to modern ocean-atmosphere forcing (Wise, 2010, 2016) and to forcings that act on millennial to glacial-interglacial timescales (Oster et al., 2015a; Hudson et al., 2019), make the site ideal for evaluating the geographic stability of this pattern on different timescales. Below we summarize the regional response to climate variability associated with D-O events during MIS 3 and 2, the overall conditions at the LGM, and the dynamic changes associated with Heinrich Events, in particular Heinrich Event 1 (HS1). We describe new insights to these patterns provided by the LSC record, including variations in both moisture source and amount as inferred from this multi-proxy record.

## 5.2.1. Dansgaard-Oeschger cycles

Multiple lake records indicate northern California and southern Oregon were characterized by wetter conditions during D-O interstadials, the warm phases of D-O events, and drier conditions during the cool phases of D-O events (Zic et al., 2002; Bradbury et al., 2004). These warm/wet and cool/dry intervals were correlated with shifts in  $\delta^{18}$ O in the Greenland ice core record but were anti-phased with climate changes recorded in Owens Lake and Lake Manix in southern California (Bradbury and Forester, 2002; Reheis et al., 2012) (Fig. 7A). Speleothem records from the southwest display positive shifts in  $\delta^{18}$ O during D-O interstadials, which are interpreted to reflect reduced winter precipitation sourced from

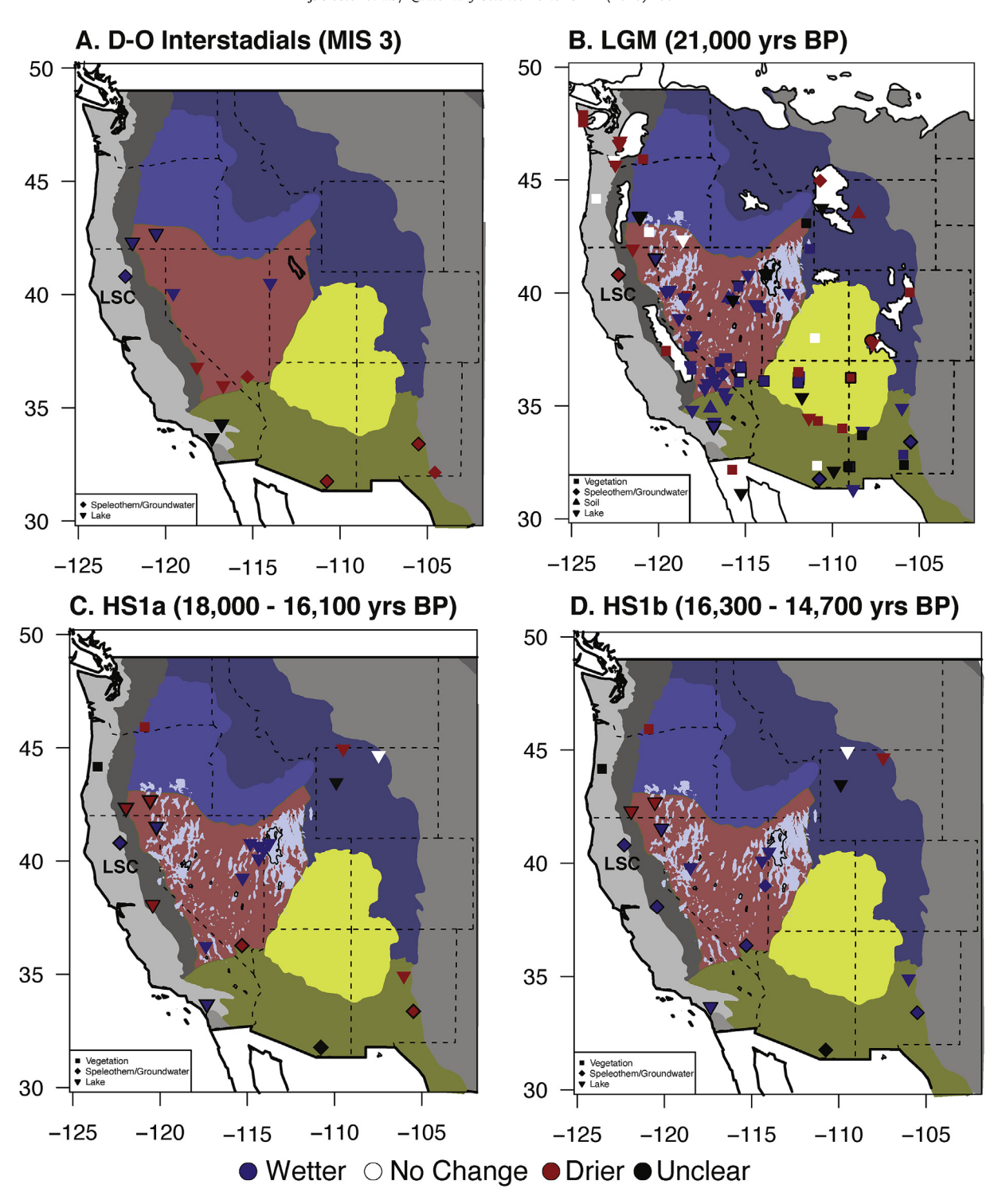


**Fig. 7.** Spatial comparison of hydrologic conditions during (A) D-O interstadials of MIS3; (B) the LGM; (C) HS1a (18,000–16,300 yrs BP); and (D) HS1b (16,300–15,000 yrs BP). Symbol color: wet (blue); dry (red); no change relative to the reference period (white), and unclear (black). For (A), hydroclimate response is assessed relative to mean MIS3 proxy values. The LGM proxy network (B), from Oster and Ibarra (2019), is assessed relative to the modern, or the Holocene for speleothem records (diamonds) that do not extend to the present. For speleothem records in (C) and (D), hydroclimate is assessed relative to the LGM. Proxies that directly assess water balance are given priority over δ<sup>18</sup>O, when available. For lake records (inverted triangles) an assessment of "wet" is given if the lake level was at its highstand or has been shown to have been rising during intervals (B), (C), and (D). For (A), lake record assessments are based on proxy evidence. Background maps show geographic regions as given in Fig. 1A. Records with bold, black outlines are shown on Fig. 1A. Proxy records included in (A), (C), and (D) are listed in Table S2. (For interpretation of the references to color in this figure legend, the reader is referred to the Web version of this article.)

the Northern Pacific during these intervals (Asmerom et al., 2010; Wagner et al., 2010) (Fig. 6).

The LSC speleothem record also suggests changes in moisture source and amount occurred in Northern California in response to millennial-scale climate changes associated with D-O events during MIS2 and 3 (Fig. 6). The LSC speleothem record shows behavior similar to that observed in the more northerly records during D-O stadials and interstadials (Fig. 7A). For example, the LSC  $\delta^{13}$ C record suggests wet conditions during D-O interstadials 3–7, similar to lake records from Klamath and Summer Lakes in southern Oregon (Zic et al., 2002; Bradbury et al., 2004). These wet intervals are coincident with the periods of erosion and/or aridisol development in the Mojave (Springer et al., 2015) (Fig. 6). The LSC  $\delta^{18}$ O record indicates that D-O interstadials are associated with increased proportions of North Pacific sourced moisture. Switches in and out of these wet periods are abrupt in our record, similar to the abrupt nature of the D-O interstadials noted in the Greenland ice core records.

A synthesis of paleoclimate records from across the southwest and Great Basin indicates a complex, spatially variable response to D-O cyclicity from MIS 5 to MIS 2 (Glover et al., 2017), though comparisons among Great Basin records are made more challenging by geochronologic uncertainties that can reach several millennia. Nonetheless, the LSC record is consistent with other northerly records that strongly suggest that a hydroclimatic dipole between the northern Great Basin and the southern Great Basin/desert southwest regions persists during the D-O cycles of MIS 3 and 2 and indicates that LSC is situated on the northern side of this precipitation dipole (Fig. 7A).

#### 5.2.2. The Last Glacial Maximum

A synthesis of hydroclimatically sensitive proxy records from across western North America illustrates a complex wet-dry dipole pattern at the LGM, with wetter than modern conditions prevailing across the Great Basin and the desert southwest and drier than modern conditions occurring closer to the Laurentide Ice Sheet in the northern Cascades, the northern Rockies, and the eastern Colorado Plateau (Fig. 7B) (Oster et al., 2015a; Oster and Ibarra, 2019). However, there is a distinct lack of proxy records that cover the LGM in Northern California. Although the LSC record does not extend to the present, the proxies suggest conditions at this site during the LGM were drier than during the preceding MIS3 and the following deglaciation. Elevated  $\delta^{13}$ C and Mg/Ca in both stalagmites support dry LGM conditions, while elevated P/Ca suggests enhanced input from the soil, perhaps due to increased erosion arising from cold, dry conditions. A geochemical and diatom-based record from Klamath Lake in Oregon, 170 km northeast of LSC indicates that the LGM was characterized by cold, dry, and windy conditions (Bradbury et al., 2004), consistent with the dry climate and hypothesized soil erosion at LSC. The Cave of the Bells speleothem record in Arizona indicates increased winter precipitation during the LGM (Wagner et al., 2010), while the Fort Stanton speleothem from New Mexico indicates enhanced winter precipitation for much of MIS2 prior to the LGM, but decreasing winter precipitation through the LGM (Asmerom et al., 2010). Pre-LGM peaks in moisture have also been noted based on initial uranium isotope records in soil opal deposits across Nevada (Maher et al., 2014), and prolonged cold and wet conditions are evident in the proxy record from Lake Elsinore in southern California beginning at 25,000 yrs BP and lasting until 15,000 yrs BP (Feakins et al., 2019) (Fig. 6). LSC  $\delta^{13}$ C values are also higher before the LGM, suggesting potentially drier conditions pre-LGM during early MIS2 (Fig. 5).

On the whole, dry conditions at LSC during the LGM also suggest that this site is associated with the northern side of the wet-dry dipole pattern, similar to what is observed through regional comparisons during D-O interstadials (Fig. 7). Climate models of 21 ka conditions associated with the PMIP2 and 3 experiments largely place the transition between wet and dry precipitation anomalies at the LGM near the location of LSC (Oster et al., 2015a). Our record suggests that this transition likely lay to the south of LSC in northern California, but additional hydrologically sensitive archives from areas to the south and east of LSC would further illuminate this pattern of hydroclimatic change. Analysis of the PMIP model output indicates that the presence of a high-pressure cell over the Laurentide Ice Sheet steered the storm track across western North America to produce the NW-SE trending dipole pattern observed in the proxy synthesis (Oster et al., 2015a; Oster and Ibarra, 2019). Further analysis of water vapor transport in the ensemble of PMIP3 models attributes the enhanced precipitation in the southwestern U.S. to increased subtropical moisture arriving via atmospheric rivers (ARs; Lora et al., 2017). The elevated  $\delta^{18}$ O in LSC3 during the LGM as compared to MIS3 and the deglacial part of the record is consistent with an increase in moisture sourced from the Central Pacific and thus consistent with the AR hypothesis (Fig. 5). However, the other LSC proxies indicate that the increase in the proportion of Central Pacific moisture was not associated with an overall increase in moisture availability. The only other speleothem  $\delta^{18}$ O records from western North America that cover the LGM and thus may be able to provide proxy evidence of the isotopic fingerprint of a shift to more subtropically-derived precipitation are the Cave of the Bells and Fort Stanton records (Oster et al., 2019). However, these southwestern sites are likely most sensitive to seasonal moisture balances between winter. Pacific-derived moisture and summer monsoon rains derived from the Gulf of Mexico. As a result, they likely do not serve as suitable recorders of changes in Pacific moisture sources (Wagner et al., 2010; Asmerom et al., 2010; Feng et al., 2014). The McLean's Cave record in the central Sierra Nevada is likely sensitive to Central versus North Pacific moisture input (Oster et al., 2015b). The MIS2 record from this cave begins at ~19,500 years BP, just overlapping the end of full glacial conditions. However, it displays relatively negative  $\delta^{18}$ O values during that time, providing no evidence for the AR hypothesis. Lastly, the Lake Elsinore leaf wax record, which remains depleted in heavy hydrogen isotopes at the LGM, indicates enhanced winter precipitation perhaps in conjunction with increased rainout along trajectories from westerly or northwesterly sources (Feakins et al., 2019). Accordingly, more coastal paleoclimate records that are specifically sensitive to the balance of Central Pacific precipitation, potentially sourced via ARs, are needed to further evaluate the influence of ARs on the LGM hydroclimate of western North America. Isotope-enabled climate models would also assist in shedding light on variations in moisture source and contribution from ARs during the LGM.

### 5.2.3. Heinrich Events

Regional syntheses of lake level high stands and other hydrologically sensitive proxies have demonstrated that the wettest conditions in western North America of the last glacial cycle did not occur at the LGM, but rather during Heinrich Stadial 1 (HS1: ~18,000 to 14,700 years BP) (e.g. Munroe and Laabs, 2013; Reheis et al., 2014). Although comparatively few paleoclimate records cover previous Heinrich stadials, available evidence indicates that these intervals were also relatively wet across western North America (McGee et al., 2018). Furthermore, lake level highstands in the northeastern part of the Great Basin occurred at the beginning of HS1, while Lake Chewaucan in the northwestern Great Basin reached its highstand after HS1 during the Bølling warm interval (Hudson et al., 2019). Lake Surprise, in northeastern California (41.5 °N), is the closest pluvial lake to LSC. The level of Lake Surprise began to rise during the first part of HS1 (HS1a) at ~17,500 years BP

and reached a highstand during the second part of HS1 (HS1b: 16,100-14,700 years BP) at ~16,000 years BP (Ibarra et al., 2014; Egger et al., 2018). This sequence of events compares favorably with the LSC proxy records, which indicate an abrupt shift to wetter conditions at ~17,500 years BP right as the level of Lake Surprise begins to increase (Fig. 6), with relatively wet conditions persisting through HS1b. However, the shift to wetter conditions in the LSC record at 17.500 vrs BP, signified by decreasing  $\delta^{13}$ C and Mg/Ca, is also accompanied by an abrupt shift to more negative  $\delta^{18}$ O values (Fig. 5). This is not consistent with enhanced subtropically derived, AR precipitation, which has been suggested as the mechanism for filling pluvial lakes (McGee et al., 2018). There is a shift to more positive  $\delta^{18}$ O that occurs in the middle of HS1 at the boundary between the HS1a and HS1b that is accompanied by an increase in  $\delta^{13}$ C and Mg/Ca. This may suggest increased Central Pacific precipitation reached northern California during this interval, possibly associated with ARs, but that it was not concurrent with the wettest conditions of HS1 at this site. The level of Lake Surprise continued to rise during this interval, reaching its highstand at the peak of the  $\delta^{18}$ O increase in the LSC record. Thus, it is possible that an increase in Central Pacific or AR precipitation contributed to the rise of Lake Surprise. However, the LSC record suggests the rise may have been begun during a period characterized by storms originating in the North Pacific.

Compared to the D-O interstadials, the LSC record and the general regional response to Heinrich Events appears to be more complex. During HS1, the initial shift to wetter conditions noted in the LSC  $\delta^{13}$ C and Mg/Ca records occurs during HS1a. This interval has been referred to as the "Big Drv" due to the recognition of a period of desiccation of Lake Estancia in New Mexico (Broecker et al., 2009; Menking et al., 2018). Recently, this period has also been described as the Extrapolar Climate Reversal (ECR) based on a comparison between Fort Stanton Cave stalagmites and various tropical and subtropical climate records (Asmerom et al., 2017). Conditions across western North America were not consistent during HS1a (Fig. 7C). The Lake Elsinore proxy records suggest wet conditions prevailed in southern California until 15,000 yrs BP (Feakins et al., 2019) (Fig. 6). Yet in the Mojave, erosion of ground water deposits suggests drier conditions (Springer et al., 2015). Further inland, highstands at Panamint Lake in southeastern California, and Bonneville, Clover, Waring, and Jakes Lakes in the eastern Great Basin were all reached during HS1a. Similar to Lake Surprise, the level of Lake Franklin in the central Great Basin was increasing from its LGM level at this time, but its highstand was not reached until later (Munroe and Laabs, 2013). In the central Sierra Nevada, speleothem trace element and  $\delta^{13}$ C records also indicate a slight drying during this interval (Fig. 6) (Oster et al., 2015b). Interestingly, although the Fort Stanton Cave  $\delta^{18}$ O record decreases (Asmerom et al., 2010, 2017), suggesting more winter precipitation in New Mexico during HS1a, speleothem  $\delta^{13}$ C and uranium isotopes suggest a slight drying at this time (Polyak et al., 2012), regionally supported by the drying event at Lake Estancia (Menking et al., 2018). The  $\delta^{18}$ O record at LSC is supportive of an influx of North Pacific moisture to the region at this time, consistent with the Fort Stanton speleothem record during the ECR, which has been linked to extratropical forcing and movement of the Intertropical Convergence Zone (Asmerom et al., 2017).

During HS1b we observe a shift to slightly drier conditions at LSC. The McLean's Cave proxy records indicate a brief shift to wetter conditions (Oster et al., 2015b) and the Lake Elsinore record and Mojave groundwater deposits indicate wet conditions persisted across southern California (Feakins et al., 2019; Springer et al., 2015). At Fort Stanton Cave, conditions remain wet, however the  $\delta^{18}$ O record suggests a shift toward less winter precipitation (Polyak et al., 2012). During this interval, lakes in the central and western

Great Basin reach high stands, including lake Franklin, Lahontan, and as previously mentioned, Lake Surprise (McGee et al., 2018; Hudson et al., 2019). On the whole, HS1b appears to be more broadly and consistently wet across western North America (Fig. 7D). This time period aligns with the interval of most reduced Atlantic Meridional Overturning Circulation (AMOC) as recorded in the <sup>231</sup>Pa/<sup>230</sup>Th ratio of deep-sea sediments in the North Atlantic (McManus et al., 2004). While the LSC record indicates very wet conditions during HS1a, HS1b remains wet compared to the LGM and even most of MIS3 (Figs. 5 and 6). North of LSC, Lake Chewaucan did not reach its highstand until ~14,000 yrs BP (Hudson et al., 2019), which is just outside of the temporal range of our record. However, conditions leading up to the Bølling appear to be wet at LSC. Similarly, cold, dry, and windy conditions appear to persist at Klamath Lake until ~15,000 yrs BP (Bradbury et al., 2004). Thus, if the dipole pattern persisted into HS1, LSC was likely influenced by wet conditions to the south to a greater degree than during the LGM or millennial-scale events of MIS3 (Fig. 7).

Heinrich events 2 and 3 are also within the timeframe of the LSC record (Fig. 7). Both are much shorter-lived than HS1 and so chronologic uncertainty makes the conditions during these intervals more challenging to evaluate. For example, during HS2, the LSC stalagmite records indicate a period of moderate conditions, where  $\delta^{13}$ C is locally lower (LSC3) or decreasing (LSC2) but overall fairly elevated relative to the MIS1 and MIS3 portions of the record, and Mg/Ca is relatively high (Fig. 5). HS3 may also be associated with a small and short-lived increase in aridity at LSC that is situated in an overall wetter period, as evidence by small peaks in  $\delta^{13}$ C and Mg/Ca. Evidence of wet conditions during Heinrich events prior to HS1 has been noted in the Great Basin and southwest (McGee et al., 2018). However, at Summer Lake (Lake Chewaucan), Heinrich Events are associated with shallower lake conditions (Zic et al., 2002). Thus, evidence from HS2 and HS3 supports the interpretation that LSC sits in a narrow transition zone, with wetter conditions to the south and drier conditions to the north, and may experience moderate drying at these times. In terms of  $\delta^{18}$ O, an increase is observed in the LSC record during HS3, but not HS2 (Fig. 5). This suggests the shift to increased Central Pacific precipitation may not be a uniform feature of Heinrich Events or may not be felt to the same degree across the region for each event.

## 6. Conclusions

In sum, records from LSC stalagmites provide novel insights into the glacial/deglacial hydroclimate of western North American as a result of their location near a long-lived hydroclimatic transition and the information they provide on moisture sources and precipitation amounts through several key paleoclimatic events from ~35,000—14,000 years BP.

The LSC record largely supports the presence of a north/south dipole in hydroclimatic response to forcings on different time-scales, indicating that this site responded in step with the Cascades, the northern Great Basin, and the Rocky Mountains during millennial-scale D-O oscillations of MIS3 and the full glacial conditions of the LGM. In contrast, HS1 was associated with wet conditions at LSC, similar to locations in the desert southwest, suggesting that the dipole's transition zone was pushed northward during this event.

The LSC record indicates spatial and temporal complexities in the role of AR precipitation in driving past wet conditions across western North America. Although LSC  $\delta^{18}$ O may in part reflect temperature shifts inside the cave, our preferred interpretation is that it indicates a shift to more Central Pacific sources of precipitation during the LGM, which is consistent with increased AR events. However, this increase in the proportion of precipitation

derived from Central Pacific sources appears to be associated with overall drier conditions at the cave. The LSC record suggests variable contributions of Central Pacific precipitation during Heinrich Events, indicating a possible increase during HS3, but not HS2. During the longer and better resolved HS1, LSC initially received enhanced amounts of North Pacific moisture coincident with the beginning of lake level increase at nearby Lake Surprise. As HS1 progressed. Lake Surprise reached a highstand coincident with a potential increase in Central Pacific moisture indicated by the LSC  $\delta^{18}$ O record. Meanwhile, the initial increase in North Pacific moisture during HS1 was associated with the wettest conditions at the cave during our records, along with contemporaneous lake level highstands in the eastern Great Basin and dry conditions in the southwest. Thus, our records suggest that during HS1 multiple moisture sources contributed to winter storms that filled pluvial lakes and influenced hydroclimatically sensitive proxies in western North America.

California's three largest freshwater reservoirs are located in its northern region and the largest, Lake Shasta, is adjacent to LSC. These reservoirs are critical components of the California water management system, supplying and storing water for much of the state. Enhanced understanding of past responses of regional rainfall to global climate perturbations provided by the new LSC record will augment the relatively brief historical record (ca. 150 years) in future efforts to predict and prepare for precipitation variability expected to accompany ongoing anthropogenic warming. Our records demonstrate that rainfall at Lake Shasta is dynamic, sensitive to the source and trajectory of Pacific winter storms, and that the reservoir is located near a critical transition between northern and southern precipitation regimes that has shifted its location in response to past external climate drivers.

#### Credit author statement

Jessica Oster: Conceptualization, Investigation, Formal Analysis, Funding acquisition, Data Curation, Writing-Original draft Isabelle Weisman: Investigation, Formal Analysis, Writing-Original draft Warren Sharp: Investigation, Resources, Validation, Writing-Review and editing.

#### Data availability

All speleothem data are archived with the NOAA Paleoclimatology Database (https://www.ncdc.noaa.gov/paleo/study/30254).

## **Declaration of competing interest**

The authors declare that they have no known competing financial interests or personal relationships that could have appeared to influence the work reported in this paper.

## Acknowledgements

JLO acknowledges support from the National Science Foundation (AGS-1554998) and the National Geographic Foundation (39815). IEW acknowledges support from the Geological Society of America. We thank David Mundt and the Lake Shasta Caverns staff for logistical help during visits to the cave and for collecting water samples, Dr. Ralf Bennartz (Vanderbilt University) for assistance with HYSPLIT analyses, Dr. Peter Blisniuk (Stanford University) and Dr. Hari Mix (Santa Clara University) for assistance with stable isotope analyses, and Christina Polito-Halter and Brian Jones (both at Berkeley Geochronology Center) for assistance with <sup>230</sup>Th/U analyses. We thank Dr. Isabel Montañez (UC Davis) and Steven

Fairchild for organizing the initial field work, and Dr. Daniel Ibarra (UC Berkeley) for further field assistance. We also thank Theresa Miller and Umang Chaudhry (both Vanderbilt University) for laboratory assistance. We acknowledge the National Air Deposition Program for providing archived precipitation samples. The authors thank the editor and two anonymous reviewers for constructive comments on this work.

## Appendix A. Supplementary data

Supplementary data to this article can be found online at https://doi.org/10.1016/j.quascirev.2020.106411.

#### References

- Asmerom, Y., Polyak, V.J., Burns, S.J., 2010. Variable winter moisture in the southwestern United States linked to rapid glacial climate shifts. Nat. Geosci. 3, 114–117.
- Asmerom, Y., Polyak, V.J., Lachniet, M.S., 2017. Extrapolar climate reversal during the last deglaciation. Sci. Rep. 7, 7157.
- Bartlein, P.J., Harrison, S.P., Brewer, S., Connor, S., Davis, B.A.S., Gajewksi, K., Guiot, J., Harrison-Prentice, T.I., Henderson, A., Peyron, O., Prentice, I.C., Scholze, M., Seppä, H., Shuman, B., Sugita, S., Thompson, R.S., Viau, A.E., Williamn, J., Wu, H., 2011. Pollen-based continental climate reconstructions at 6 and 21 ka: a global synthesis. Clim. Dynam. 37, 775–802.
- Belli, R., Borsato, A., Frisia, S., Drysdale, R., Maas, R., Greig, A., 2017. Investigating the hydrological significance of stalagmite geochemistry (Mg, Sr) using Sr isotope and particulate element records across the Late Glacial-to-Holocene transition. Geochem. Cosmochim. Acta 199, 247–263.
- Benson, L.V., Smoot, J.P., Lund, S.P., Mensing, S.A., Foit, F.F., Rye, R.O., 2013. Insights from a synthesis of old and new climate-proxy data from the Pyramid and Winnemucca lake basins for ther period 48 11.5 cal. ka., 2013. Quat. Int. 310, 62–82
- Berkelhammer, M., Stott, L., Yoshimura, K., Johnson, K., Sinha, A., 2012. Synoptic and mesoscale controls on the isotopic composition of precipitation in the western United States. Clim. Dynam. 38, 433–454.
- Borsato, A., Frisia, S., Fairchild, I.J., Somogyi, A., Susini, J., 2007. Trace element distribution in annual stalagmite laminae mapped by micrometer-resolution X-ray fluorescence. Implications for incorporation of environmentally significant species. Geochem. Cosmochim. Acta 71, 1494–1512.
- Bradbury, J.P., Colman, S.M., Dean, W.E., 2004. Limnological and climatic environments at Upper Klamath Lake, Oregon during the past 45000 years. J. Paleolimnol. 31, 167–188.
- Bradbury, J.P., Forester, R.M., 2002. Environment and paleolimnology of Owens Lake, California: a record of climate and hydrology for the past 50,000 years. In: Hershler, R., Madsen, D.B., Currey, D.R. (Eds.), Great Basin Aquatic System History, vol. 33. Smithsonian Contributions to the Earth Sciences, pp. 145–173.
- Breecker, D., 2017. Atmospheric pCO<sub>2</sub> control on speleothem stable carbon isotope compositions. Earth Planet Sci. Lett. 458, 58–68.
- Briles, C.E., Whitlock, C., Bartlein, P.J., 2005. Postglacial vegetation, fire, and climate history of the Siskiyou Mountains, Oregon, USA. Quat. Res. 64, 44–56.
- Broecker, W.S., McGee, D., Adams, K., Cheng, H., Edwards, R.L., Oviatt, C.G., Quade, J., 2009. A Great Basin-wide dry episode during the first half of the mystery interval? Ouat. Sci. Rev. 28, 2557–2563.
- Busenberg, E., Plummer, L.N., 1989. Thermodynamics of magnesian calcite solidsolutions at 25°C and 1 atm total pressure. Geochem. Cosmochim. Acta 53, 1189—1208.
- Cheng, H., Edwards, R.L., Shen, C.-C., et al., 2013. Improvements in <sup>230</sup>Th dating, <sup>230</sup>Th and <sup>234</sup>U half-life values, and U-Th isotopic measurements by multi-collector inductively coupled plasma mass spectrometry. Earth Planet Sci. Lett. 371–372, 82–91.
- Cheng, H., Edwards, R.L., Sinha, A., Spötl, C., Yi, L., Chen, S., Kelly, M., Kathayat, G., Wang, X., Li, X., Kong, X., Wang, Y., Ning, Y., Zhang, H., 2016. The Asian monsoon over the past 640,000 years and ice age terminations. Nature 534, 640–646.
- Chou, K., Garrels, R.M., Wollast, R., 1989. Comparative study of the kinetics and mechanisms of dissolution of carbonate minerals. Chem. Geol. 78, 269–282.
- Demirmen, F., Harbaugh, J.W., 1965. Petrography and origin of permian McCloud limestone of northern California. J. Sediment. Petrol. 35, 136–154.
- Dettinger, M.D., Cayan, D.R., Diaz, H.F., Meko, D.M., 1998. North-south precipitation patterns in western North America on annual to decadal timescales. J. Clim. 11, 3095—3111.
- Dettinger, M., 2004. Fifty-two years of "pineapple express" storms across the west coast of North America. U.S. Geological survey, scripps institution of oceanography for the California energy commission. In: PIER Energy-Related Environmental Research. CEC-500-2005-004.
- Dorale, J.D., Liu, D., 2009. Limitations of Hendy Test criteria in judging the paleoclimatic suitability of speleothems and the need for replication. J. Cave Karst Stud. 71, 73–80.
- Egger, A.E., Ibarra, D.E., Widden, R., Landgridge, R.M., Marion, M., Hall, J., 2018. Influence of Pluvial Lake Cycles on Earthquake Recurrence in the Northwestern

- Basin and Range, vol. 536. Geological Society of America Special Paper, USA, pp. 1–28.
- Ersek, V., Mix, A.C., Clark, P.U., 2010. Variations in rainwater from southwestern Oregon. J. Geophys. Res. 115, D09109. https://doi.org/10.1029/2009/D013345.
- Ersek, V., Clark, P.U., Mix, A.C., Cheng, H., Edwards, F.L., 2012. Holocene winter climate variability. Nat. Commun. 3, 1219. https://doi.org/10.1038/ncomms2222.
- Fairchild, I.J., Borsato, A., Tooth, A.F., Frisia, S., Hawkesworth, C., Huang, Y., McDermott, F., Spiro, B., 2000. Controls on trace element (Sr-Mg) compositions of carbonate cave waters: implications for speleothem climatic records. Chem. Geol. 166, 255–269.
- Feakins, S.J., Wu, M.S., Ponton, C., Tierney, J.E., 2019. Biomarkers reveal abrupt switches in hydroclimate during the last glacial in southern California. Earth Planet Sci. Lett. 515, 164–172.
- Feng, W., Hardt, B., Banner, J.L., Meyer, K.J., James, E.W., Musgrove, M., Edwards, R.L., Cheng, H., Min, A., 2014. Changing amounts and sources of moisture in the U.S. southwest since the Last Glacial Maximum in response to global climate change. Earth Planet Sci. Lett. 401, 47–56.
- Fohlmeister, J., 2012. A statistical approach to construct composite climate records of dated archives. Quat. Geochronol. 14, 48–56.
- Fohlmeister, J., Voarinstsoa, N.R.G., Lechleitner, F.A., Boyd, M., Brandstätter, Jacobson, M.J., Oster, J.L., 2020. Main controls on the stable carbon isotope composition of speleothems. Geochem. Cosmochim. Acta. https://doi.org/10.1016/j.gca.2020.03.042 (in press).
- Fraticelli, L.A., Albers, J.P., Irwin, W.P., Blake, M.C., Wentworth, C.M., 2012. Digital Geologic Map of the Redding 1° X 2 ° Degree Quadrangle, Shasta, Tehama, Humboldt, and Trinity Counties. USGS Open-File, California. Report 2012-1228.
- Friedman, I.G., Smith, I., Gleason, J., Warden, A., Harris, J.M., 1992. Stable isotope composition of precipitation in southeastern California, 1, Modern precipitation. J. Geophys. Res. 97, 5795—5812.
- Glover, K.G., MacDonald, G.M., Kirby, M.E., Rhodes, E.J., Stevens, L., Silveira, E., Whitaker, A., Lydon, S., 2017. Evidence for orbital and North Atlantic climate forcing in alpine Southern California between 125 and 10 ka from multi-proxy analyses of Baldwin Lake. Quat. Sci. Rev. 167, 47–62.
- Hartland, A., Fairchild, I.J., Lead, J.R., et al., 2012. From soil to cave: transport of trace metals by natural organic matter in karst dripwaters. Chem. Geol. 304–305, 68–82.
- Holden, N.E., 1989. Total and spontaneous fission half-lives for uranium, plutonium, americium, and curium nuclides. Pure Appl. Chem. 61, 1483–1504.
- Hudson, A.M., Quade, J., Ali, G., Boyle, D., Bassett, S., Huntington, K.W., De los Santos, M., Cohen, A.S., Lin, K., Wang, X., 2017. Stable C, O and clumped isotope systematics and 14C geochronology of carbonates from the Quaternary Chewaucan closed-basin lake system, Great Basin, USA: implications for paleoenvironmental reconstructions using carbonates. Geochem. Cosmochim. Acta 212, 274–302.
- Hudson, A.M., Hatchett, B.J., Quade, J., Boyle, D.P., Bassett, S.D., De los Santos, M.G., 2019. North-south dipole in winter hydroclimate in the western United States during the last deglaciation. Sci. Rep. 9, 4826. https://doi.org/10.1038/s41598-019-41197-y.
- Ibarra, D.E., Egger, A.E., Weaver, K.L., Harris, C.R., Maher, K., 2014. Rise and fall of late Pleistocene pluvial lakes in response to reduced evaporation and precipitation: evidence from Lake Surprise, California. Geol. Soc. Am. Bull. 126, 1387–1415. https://doi.org/10.1130/B31014.1.
- Jaffey, A.H., Flynn, K.F., Glendeinin, L.E., Bentley, W.C., Essling, A.M., 1971. Precise measurement of half-lives and specific activities of <sup>235</sup>U and <sup>238</sup>U. Phys. Rev. C 4, 1899–1906.
- Jiang, P., Yu, Z., Gautam, M.R., 2013. Pacific and Atlantic Ocean influences on the spatiotemporal variability of heavy precipitation in the western United States. Global Planet. Change 109, 38–45.
- Lê, S., Josse, J., Husson, F., 2008. FactoMineR: an R package for multivariate analysis. J. Stat. Software 25, 1–18.
- Lora, J.M., Mitchell, J.L., Risi, C., Tripati, A.E., 2017. north Pacific atmospheric rivers and their influence on western North America at the last glacial maximum. Geophys. Res. Lett. 44, 1051–1059. https://doi.org/10.1002/2016GL071541.
- Maher, K., Ibarra, D.E., Oster, J.L., Miller, D.M., Redwine, J.L., Reheis, M.C., Harden, J.W., 2014. Uranium isotopes in soils as a proxy for past infiltration and precipitation across the western United States: Am. J. Sci. 314, 821–857.
- McCabe-Glynn, S., Johnson, K.R., Strong, C., Zou, Y., Yu, J.-Y., Sellars, S., Welker, J.M., 2016. Isotopic signature of extreme precipitation events in the western U.S. and associated phases of Arctic and tropical climate modes. J. Geophys. Res.: Atmosphere 121, 8913–8924. https://doi.org/10.1002/2016JD025524.
- McGee, D., Moreno-Chamarro, E., Marshall, J., Galbraith, E.D., 2018. Western U.S. lake expansions during Heinrich stadials linked to Pacific Hadley circulation. Sci. Adv. 4 eaav0118.f.
- McManus, J.F., Francois, R., Gherardi, J.-M., Keigwin, L.D., Brown-Leger, S., 2004. Collapse and rapid resumption of Atlantic meridional circulation linked to deglacial climate changes. Nature 428, 834.
- Menking, K., Polyak, V.J., Anderson, R.Y., Asmerom, Y., 2018. Climate history of the southwestern United States based on Estancia Basin hydrologic variability from 69 to 10 ka. Quat. Sci. Rev. 200, 237–252.
- Merlivat, L., Jouzel, J., 1979. Global climatic interpretation of the deuterium-oxygen 18 relationship for precipitation. J. Geophys. Res. Atmos. 84 (C8), 5029–5033.
- Mickler, P.J., Banner, J.L., Stern, L., et al., 2004. Stable isotope variations in modern tropical speleothems: evaluating equilibrium vs. kinetic isotope effects. Geochem. Cosmochim. Acta 68, 4381–4393.

- Morrill, C., Lowry, D.P., Hoell, A., 2018. Thermodynamic and dynamic causes of pluvial conditions during the Last Glacial Maximum in western North America. Geophys. Res. Lett. 45, 335–345.
- Munroe, J.S., Laabs, B.J.C., 2013. Temporal correspondence between pluvial lake highstands in the southwestern US and Heinrich Event 1. J. Quat. Sci. 28, 49–58. https://doi.org/10.1002/jqs2586.
- Oster, J.L., Ibarra, D.E., Winnick, M.J., Maher, K., 2015a. Steering of westerly storms over western North America at the last glacial maximum. Nat. Geosci. 8, 201–205. https://doi.org/10.1038/ngeo2365.
- Oster, J.L., Ibarra, D.E., 2019. Glacial hydroclimate of western North America: insights from proxy-model comparison and implications for Lake Bonneville. In: Lund, W.R., McKean, A.P., Bowman, S.D.( (Eds.), Proceedings Volume: 2018 Lake Bonneville Geologic Conference and Short Course, vol. 170. Utah Geological Survey Miscellaneous Publication.
- Oster, J.L., et al., 2015b. Stalagmite records of hydroclimate in central California during Termination 1. Quat. Sci. Rev. 127, 199–214.
- Oster, J.L., Kelley, N.P., 2016. Tracking regional and global teleconnections recorded by western North American speleothem records. Quat. Sci. Rev. 149, 18–33.
- Oster, J.L., Montañez, I.P., Kelley, N.P., 2012. Response of a modern cave system to large seasonal precipitation variability. Geochem. Cosmochim. Acta 91, 92–108.
- Oster, J.L., Montañez, I.P., Mertz-Krause, R., et al., 2014. Millennial-scale variations in western Sierra Nevada precipitation during the last glacial cycle MIS 4/3 transition. Quat. Res. 82, 236–248.
- Oster, J.L.J., Sharp, W.D., Covey, A.K., Gibson, J., Rogers, B., Mix, H., 2017. Climate response to the 8.2 kyr event in Coastal California. Sci. Rep. 7, 3886. https://doi.org/10.1038/s41598-017-04215-5.
- Oster, J.L., Warken, S.E., Sekhon, N., Arienzo, M.M., Lachniet, M., 2019. Speleothem paleoclimatology for the Caribbean, Central America, and North America. Quaternary 2 (3). https://doi.org/10.3390/quat2010005.
- Polyak, V., Asmerom, Y., Burns, S.J., Lachniet, M.S., 2012. Climatic backdrop to the terminal Pleistocene extinction of North American mammals. Geology. https:// doi.org/10.1130/G33226.1.
- Reheis, M.C., Bright, J., Lund, S.P., Miller, D.M., Skipp, G. Fleck, 2012. A half-millionyear record of paleoclimate from the lake Manix core, Mojave Desert, California. Palaeogeogr. Palaeoclimatol. Palaeoecol. 365–366, 11–37.
- Redmond, K.T., Koch, R.W., 1991. Surface climate and streamflow variability in the western United States and their relationship to large-scale circulation indices. Water Resour. Res. 27, 2381–2399.
- Reheis, M.C., Adams, K.D., Oviatt, C.G., Bacon, S.N., 2014. Pluvial lakes of the western United States a view from the outcrop. Quat. Sci. Rev. 97, 33—37.
- Rutlidge, H., Baker, A., Marjo, C.E., Andersen, M.S., Graham, P.W., Cuthbert, M.O., Rau, G.C., Roshan, H., Markowska, M., Mariethoz, G., Jex, C., 2014. Dripwater organic matter and trace element geochemistry in a semi-arid karst environment: implications for speleothem paleoclimatology. Geochem. Cosmochim. Acta 135, 217–230.
- Scheff, J., Seager, R., Liu, H., Coats, S., 2017. Are glacials dry? Consequences for paleoclimatology and for greenhouse warming, J. Clim. 30, 6593–6609.
- Sinclair, D., Banner, J.L., Taylor, F.W., Partin, J., Jenson, J., Mylroie, J., Goddard, E., Quinn, T., Jocson, J., Miklavic, B., 2012. Magnesium and strontium systematics in tropical speleothems from the Western Pacific. Chem. Geol. 294–295, 1–17.
- Springer, K.B., Manker, C.R., Pigati, J.S., 2015. Dynamic response of desert wetlands to abrupt climate change. Proc. Natl. Acad. Sci. Unit. States Am. 112, 14522–14526.
- Stein, A.F., Draxler, R.R., Rolph, G.D., Stunder, B.J.B., Cohen, D., Ngan, F., 2015. NOAA's HYSPLIT atmospheric transport and dispersion mdeling system. Bull. Amer. Meteor. Soc. 96, 2059–2077. https://doi.org/10.1175/BAMS-D-14-00110.1.
- Steponaitis, E., Andrews, A., McGee, D., et al., 2015. Mid-Holocene drying of the U.S. Great Basin recorded in Nevada speleothems. Quat. Sci. Rev. 127, 174–185.
- Tremaine, D.M., Froelich, P.N., Wang, Y., 2011. Speleothem calcite farmed in situ: modern calibration of  $\delta^{18}$ O and  $\delta^{13}$ C paleoclimate proxies in a continuously-monitored natural cave system. Geochem. Cosmochim. Acta 75, 4929–4950.
- Svensson, A.K., Andersen, K., Bigler, M., Clausen, H.B., Dahl-Jensen, D., Davies, S.M., Johnsen, S.J., Muscheler, R., Parrenin, F., Rasmussen, S.O., Röthisberger, R., Seierstad, I., Steffensen, J.P., Vinther, B.M., 2008. A 60,000 year Greenland stratigraphic ice core record. Clim. Past 4, 47–57.
- Thompson, R.S., Whitlock, C., Bartlein, P.J., Harrison, S.P., Spaulding, W.G., 1993. Climatic changes in the western United States since 18,000 yr BP. In: Wright Jr., H.E., Kutzbach, J.E., Webb III, T., Street-Perrott, F.E., Bartlein, P.J. (Eds.), Global Climates since the Last Glacial Maximum. University of Minnesota Press, Minneapolis, pp. 468–513.
- Tremaine, D.M., Froelich, P.N., 2013. Speleothem trace element signatures: a hydrologic geochemical study of modern cave dripwaters and farmed calcite. Geochem. Cosmochim. Acta 121, 522–545.
- Vachon, R., Welker, J., White, J., Vaughn, B., 2010. Moisture source temperatures and precipitation  $\delta^{18}$ O-temperature relationships across the United States. Water Resour. Res. 46 (7), W07523.
- Wagner, J.D.M., Cole, J.E., Beck, J.W., Patchett, P.J., Henderson, G.M., Barnett, H.R., 2010. Nat. Geosci. 3, 110–113.
- Wand, M., 2019. KernSmooth: functions for Kernel Smoothing Supporting Wand and Jones (1995). R package version 2.23-16. https://CRAN.R-project.org/package—KernSmooth.
- Wise, E.K., 2010. Spatiotemporal variability of the precipitation dipole transition zone in the western United States. Geophys. Res. Lett. 37, L07706.
- Wise, E.K., 2016. Five centuries of U.S. West Coast drought: occurrence, spatial

distribution, and associated atmospheric circulation patterns. Geophys. Res. Lett. 43, 4539–4546.

Wolff, E.W., Chappellaz, J., Blunier, T., Rasmussen, S.O., Svensson, A., 2010. Millennial-scale variability during the last glacial: the ice core record. Quat. Sci. Rev.

29, 2828–2838.

Zic, M., Negrini, R.M., Wigand, P., 2002. Evidence of synchronous climate change across the Northern hemisphere between the north Atlantic and the northwestern Great Basin, United States. Geology 30, 635–638.